NUREG/CR-1941
ORNL/NUREG/TM-437
Dist. Category RF

Contract No. W-7405-eng-26

Engineering Technology Division

HEAVY-SECTION STEEL TECHNOLOGY PROGRAM QUARTERLY PROGRESS REPORT FOR OCTOBER–DECEMBER 1980

G. D. Whitman R. H. Bryan

Manuscript Completed – March 5, 1981
Date Published – March 1981

Prepared for the
U.S. Nuclear Regulatory Commission
Office of Nuclear Regulatory Research
Under Interagency Agreements DOE 40-551-75 and 40-552-75

NRC FIN No. B0119

Prepared by the
OAK RIDGE NATIONAL LABORATORY
Oak Ridge, Tennessee 37830
operated by
UNION CARBIDE CORPORATION
for the
DEPARTMENT OF ENERGY

CONTENTS

PREFACE

The Heavy-Section Steel Technology (HSST) Program, which is sponsored by the Nuclear Regulatory Commission is an engineering research activity devoted to extending and developing the technology for assessing the margin of safety against fracture of the thick-walled steel pressure vessels used in light-water-cooled nuclear power reactors. The program is being carried out in close cooperation with the nuclear power industry. This report covers HSST work performed in October through December 1980. The work performed by Oak Ridge National Laboratory (ORNL) and by subcontractors is managed by the Engineering Technology Division. Major tasks at ORNL are carried out by the Engineering Technology Division and the Metals and Ceramics Division. Prior progress reports on this program are ORNL-4176, ORNL-4315, ORNL-4377, ORNL-4463, ORNL-4512, ORNL-4590, ORNL-4653, ORNL-4681, ORNL-4764, ORNL-4816, ORNL-4855, ORNL-4918, ORNL-4971, ORNL/TM-4655 (Vol. II), ORNL/TM-4729 (Vol. II), ORNL/TM-4805 (Vol. II), ORNL/TM-4914 (Vol. II), ORNL/TM-5021 (Vol. II), ORNL/TM-5170, ORNL/NUREG/TM-3, ORNL/NUREG/TM-28, ORNL/NUREG/TM-49, ORNL/NUREG/TM-64, ORNL/NUREG/TM-94, ORNL/NUREG/TM-120, ORNL/NUREG/TM-147, ORNL/NUREG/TM-166, ORNL/NUREG/TM-194, ORNL/NUREG/TM-209, ORNL/NUREG/TM-239, NUREG/CR-0476 (ORNL/NUREG/TM-275), NUREG/CR-0656 (ORNL/NUREG/TM-298), NUREG/CR-0818 (ORNL/NUREG/TM-324), NUREG/CR-0980 (ORNL/NUREG/TM-347), and NUREG/CR-1197 (ORNL/NUREG/TM-370), NUREG/CR-1305 (ORNL/NUREG/TM-380), NUREG/CR-1477 (ORNL/NUREG/TM-393), NUREG/CR-1627 (ORNL/NUREG/TM-401), and NUREG/CR-1806 (ORNL/NUREG/TM-419).

SUMMARY

1. PROGRAM ADMINISTRATION AND PROCUREMENT

The Heavy-Section Steel Technology (HSST) Program is an engineering research activity conducted by the Oak Ridge National Laboratory (ORNL) for the Nuclear Regulatory Commission (NRC) in coordination with other research sponsored by the federal government and private organizations. The program comprises studies related to all areas of the technology of materials fabricated into thick-section primary-coolant containment systems of light-water-cooled nuclear power reactors. The principal area of investigation is the behavior and structural integrity of steel pressure vessels containing cracklike flaws. Current work is organized into the following tasks: (1) program administration and procurement, (2) fracture mechanics analyses and investigations, (3) investigations of irradiated materials, (4) thermal shock investigations, and (5) pressure vessel investigations.

The work performed under the existing research and development subcontracts is included in this report.

Ten program briefings, reviews, or presentations were made during the quarter.

2. FRACTURE MECHANICS ANALYSES AND INVESTIGATIONS

The plate and cylinder options of the finite-element computer program OR-FLAW have been made fully operational on the IBM computers at Union Carbide Corporation Nuclear Division. This program is being tested for use in calculating stress-intensity factors K_I for finite surface flaws in cylinders under combined pressure and thermal loads. Comparisons were made with previous K_I calculations by the ADINA program for pressure only.

At the University of Maryland, studies of ductile-brittle transition in fracture are continuing in cooperation with other laboratories. As an adjunct to these studies, and investigation is being made of the importance of nonsingular stress field terms in the determination of K_I by photoelastic experiments.

3. INVESTIGATIONS OF IRRADIATED MATERIALS

The remaining Charpy V-notch impact specimens from the Second and Third 4T-CTS Irradiation Studies were tested.

In the Fourth HSST Irradiation Series, the irradiation of capsule A was completed. Irradiation of capsule B continued through the quarter.

4. THERMAL SHOCK INVESTIGATIONS

A preliminary posttest analysis of thermal-shock experiment TSE-5A was completed. Four initiation-arrest events were observed. The effectiveness of warm prestressing in preventing initiation of a deep flaw was conclusively demonstrated. Arrest in a rising K_I field was demonstrated. The effective fracture initiation and arrest toughnesses of the test cylinder were significantly less than the values derived from pretest characterization studies.

A computer program for static two-dimensional linear-elastic fracture mechanics analysis of a pressurized-water reactor vessel under thermal-pressure transient loading was written and made operational at Oak Ridge National Laboratory.

5. PRESSURE VESSEL INVESTIGATIONS

In preparation for testing intermediate vessel V-8A with the flaw in a low-upper-shelf seam weld, the final trial weld was made; tensile, Charpy-V impact, and J-R curve specimens were tested. The trial weld met specifications, and the decision was made to proceed with vessel preparation with the procedure used in the trial weld.

Studies of pressurized-thermal-shock testing concepts have led to the current consideration of such tests being conducted with outside surface flaws in the cylindrical section of intermediate test vessels. Tests in which the outside surface is thermally shocked have several advantages over the earlier concepts of shocking the inside nozzle-corner region.

HEAVY-SECTION STEEL TECHNOLOGY PROGRAM QUARTERLY PROGRESS REPORT FOR OCTOBER–DECEMBER 1980

G. D. Whitman R. H. Bryan

ABSTRACT

The Heavy-Section Steel Technology (HSST) Program is an engineering research activity conducted by the Oak Ridge National Laboratory for the Nuclear Regulatory Commission. The program comprises studies related to all areas of the technology of materials fabricated into thick-section primary-coolant containment systems of light-water-cooled nuclear power reactors. The investigation focuses on the behavior and structural integrity of steel pressure vessels containing cracklike flaws. Current work is organized into five tasks: (1) program administration and procurement, (2) fracture mechanics analyses and investigations, (3) investigations of irradiated materials, (4) thermal shock investigations, and (5) pressure vessel investigations.

A finite-element computer program is operational for direct calculation of stress-intensity factors of surface flaws in cylinders, nozzle corners, and plates. Studies of ductile-brittle transition in fracture are continuing. Irradiation of one capsule in the Fourth HSST Irradiation Series was completed, and irradiation of the second capsule is continuing. Posttest analysis of thermal shock experiment TSE-5A indicates that all major objectives were attained. Properties of the trial weld for intermediate test vessel V-8A were satisfactory, and preparations for the vessel test were continued. Studies of pressurized-thermal-shock testing concepts are proceeding.

---

1. PROGRAM ADMINISTRATION AND PROCUREMENT

G. D. Whitman

The Heavy-Section Steel Technology (HSST) Program, a major safety program sponsored by the Nuclear Regulatory Commission (NRC) at the Oak Ridge National Laboratory (ORNL), is concerned with the structural integrity of the primary systems (particularly the reactor pressure vessels) of light-water-cooled nuclear power reactors. The structural integrity of these vessels is ensured by (1) designing and fabricating them according to standards set by the code for nuclear pressure vessels, (2) detecting flaws of significant size that occur during fabrication and in service, and (3) developing methods of producing quantitative estimates of conditions under which fractures could occur. The program is concerned mainly with developing pertinent fracture technology, including knowledge of (1) the material used in these thick-walled vessels, (2) the flaw growth

rate, and (3) the combination of flaw size and load that would cause fracture and thus limit the life and/or operating conditions of this type of reactor plant.

The program is coordinated with other government agencies and with the manufacturing and utility sectors of the nuclear power industry in the United States and abroad. The overall objective is a quantification of safety assessments for regulatory agencies, for professional code-writing bodies, and for the nuclear power industry. Several activities are conducted under subcontracts by research facilities in the United States and through informal cooperative efforts on an international basis. The subcontract with Materials Research Laboratory expired at the end of the previous quarter, and subcontract work by Battelle Memorial Institute (Columbus) was instituted during the current quarter. Two research and development subcontracts are currently in force.

Administratively, the program is organized into five tasks, as reflected in this report: (1) program administration and procurement, (2) fracture mechanics analyses and investigations, (3) investigations of irradiated material, (4) thermal shock investigations, and (5) pressure vessel investigations.

During this quarter, 10 program briefings, reviews, or presentations were made by the HSST staff at technical meetings and at program reviews for the NRC staff or visitors.

2. FRACTURE MECHANICS ANALYSES AND INVESTIGATIONS*

2.1 A Computer Program (OR-FLAW) for Direct Evaluation of K-Factors for User-Defined Flaws in Plates, Cylinders, and Pressure Vessel Nozzle Corners

B. R. Bass† J. W. Bryson

During this quarter, the plate and cylinder options of the NOZ-FLAW finite-element computer program were made fully operational in the Union Carbide Corporation Nuclear Division (UCCND) computer facility. In addition to the nozzle-corner-flaw configurations reported previously,[1,2] the program is now capable of automatically generating finite-element meshes and calculating K-distributions for the plate, plate-hole, and cylinder configurations shown in Figs. 2.1, 2.2, and 2.3, respectively. Because the nozzle-corner-flaw option is only one of 21 possible options available to a user, the program has been renamed OR-FLAW (Oak Ridge-FLAW) to reflect this generality. Any combination of several different types of loading (including thermal shock) may be employed for each option, that is, flaw configuration. Either mathematical or user-defined flaw shapes may be considered. A user's manual for the nozzle-corner-flaw option[2] of OR-FLAW has gone to the printer, and work will be initiated shortly on a draft of a second manual to give user instructions for the plate and cylinder options.[3]

2.2 Determination of K-Factors for Surface Flaws in Cylinders Under Combined Pressure-Thermal Loading

J. W. Bryson B. R. Bass R. H. Bryan

The K_I distributions for a part-circular flaw on the outside surface of a cylindrical vessel (ITV V-8) under combined loadings are being calculated using the OR-FLAW[3] and ADINAT[4] finite-element codes. This work is analogous to that reported earlier[5] for nozzle-corner flaws where the ADINAT, ADINA,[6] and BIGIF[7] codes were used. Figures 2.4 and 2.5 show the dimensions of a quarter-section of the cylinder as modeled and the finite-element discretization used in the plane of the flaw. The OR-FLAW code employs special crack-tip elements (marked S) that have the proper square root and inverse square root variations for displacements and stresses, respectively. The remaining elements are regular 20-node isoparametric brick elements. Figure 2.6 gives the OR-FLAW K_I distribution along the flaw front for an internal pressure loading of 68.9 MPa. A previously reported K_I distribution for the same flaw configuration using ADINA and a

*Conversions from SI to English units for all SI quantities are listed on a foldout page at the end of this report.

†Computer Sciences Division, UCCND.

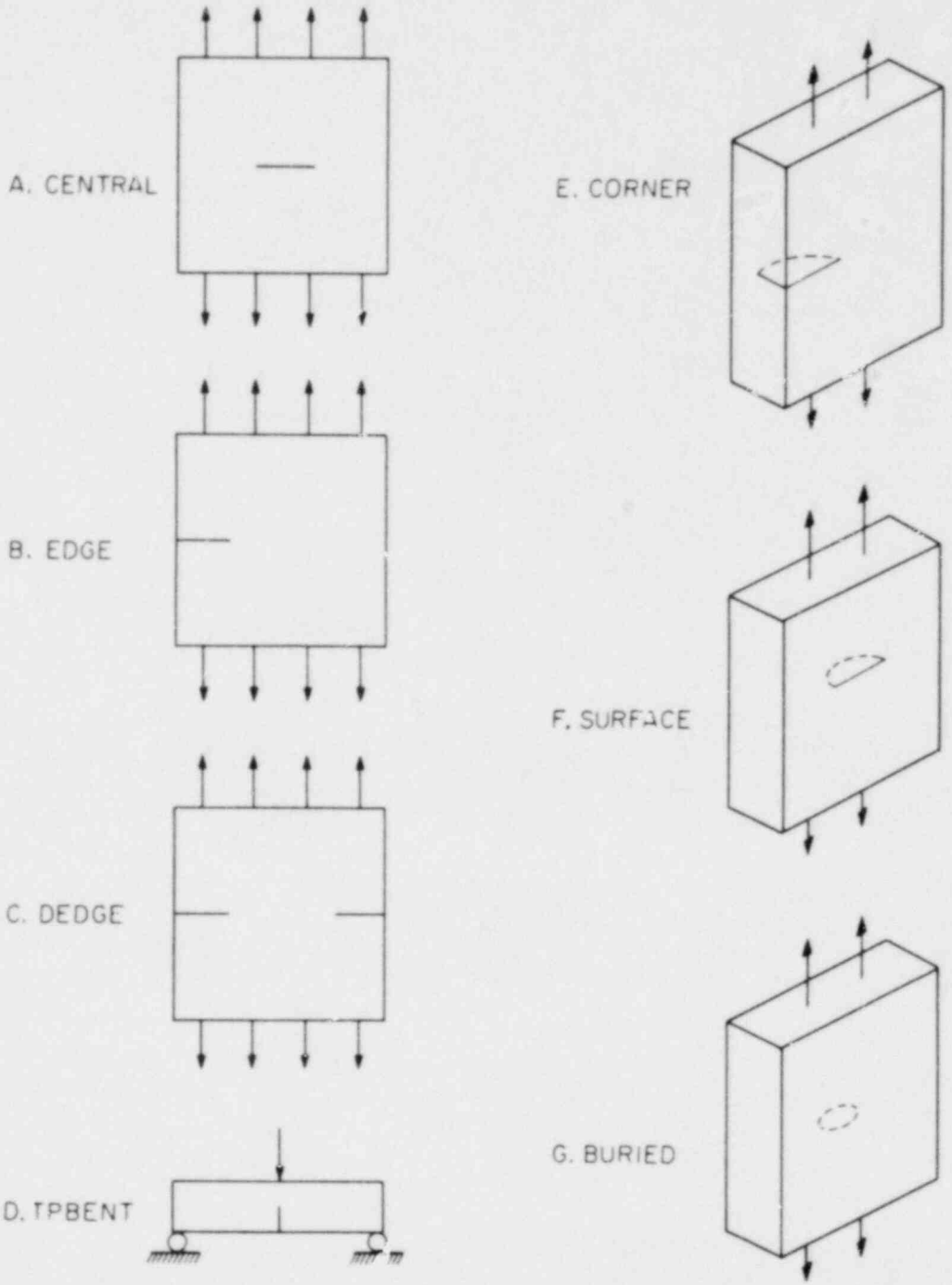

Fig. 2.1. Flat-plate flaw configurations available in OR-FLAW.

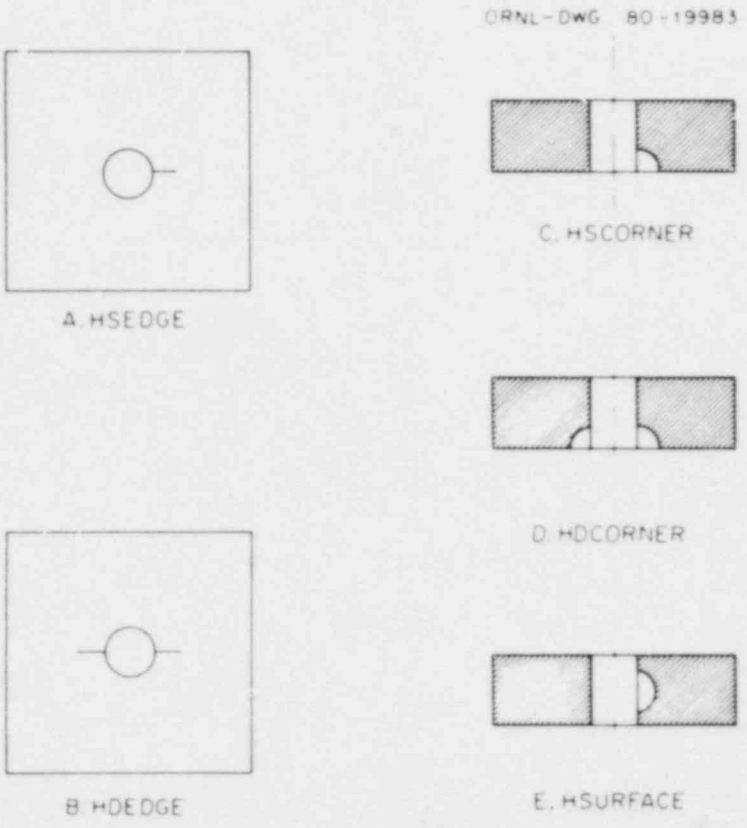

Fig. 2.2. Plate-hole flaw configurations available in OR-FLAW.

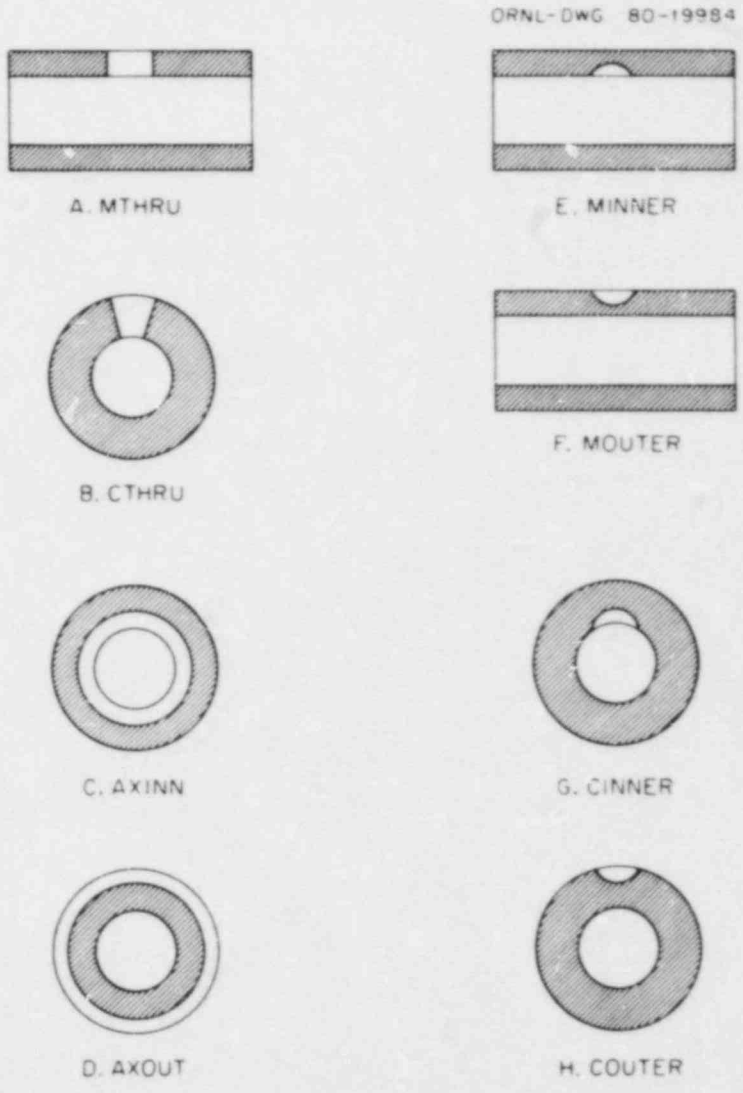

Fig. 2.3. Cylinder flaw configurations available in OR-FLAW.

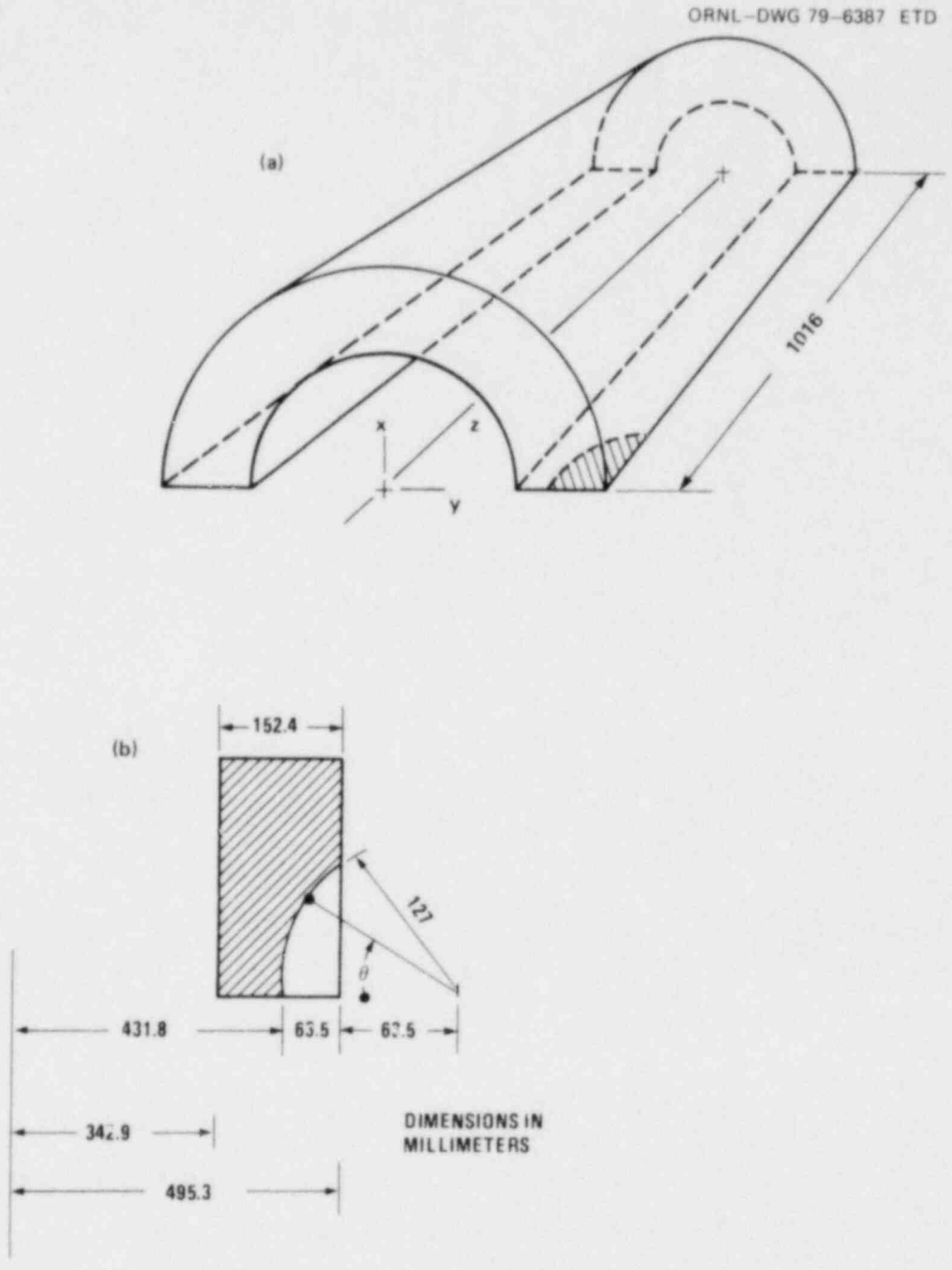

Fig. 2.4. Description of V-8 cylinder analyzed showing flaw and quarter cylinder as modeled.

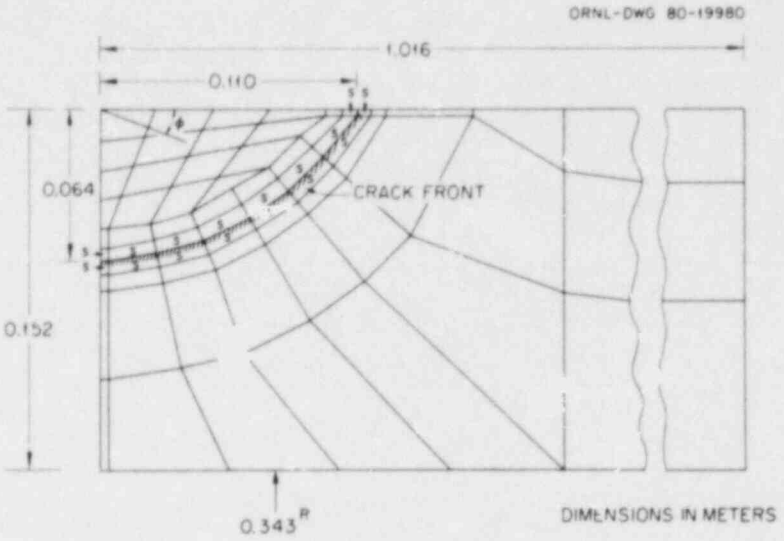

Fig. 2.5. OR-FLAW finite-element discretization for V-8 surface flaw showing special crack-tip elements along flaw front.

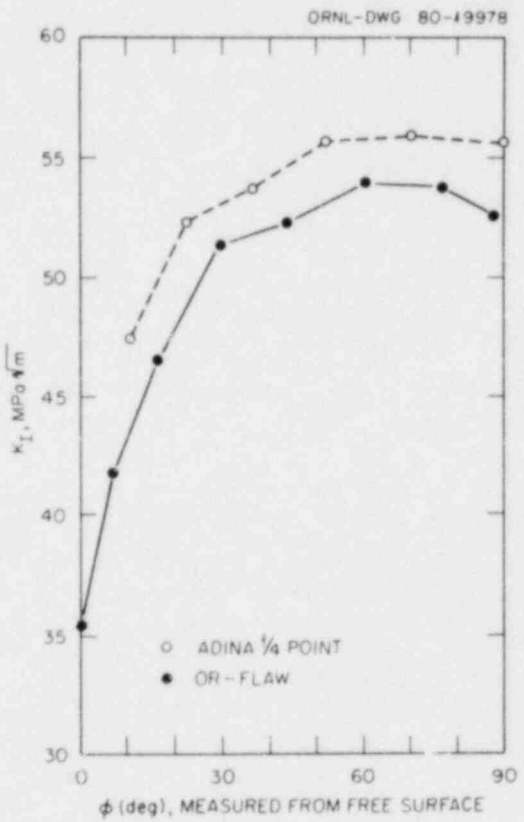

Fig. 2.6. Calculated K_I distributions for V-8 surface flaw (p = 68.9 MPa).

quarter-point technique is also shown.[8,9] Work is currently under way to determine K_I distributions for a combined thermal shock applied to the outside surface and an internal pressure loading.

2.3 Computational Methods for Elastic-Plastic Fracture Mechanics

B. R. Bass J. W. Bryson

Work was initiated this quarter to implement into the Oak Ridge version of the ADINA[6] finite-element code a procedure for the calculation of the J-integral at each load step during a step-by-step elastic-plastic calculation. This procedure is described in detail in Ref. 10 and outlined briefly in the following paragraphs. Eight-noded two-dimensional (2-D) isoparametric elements are used in the modeling, and up to ten integration paths may be taken around the crack tip. For each load step, each element along an integration path contributes an increment to the J-integral. The integration paths traverse through Gauss points to facilitate the numerical integration (Gaussian quadrature). Figures 2.7 and 2.8 show an element and illustrate paths straight across and turning in an element for a 3 × 3 integration scheme.

The necessary modifications to ADINA have been performed, and check cases are presently being run. Because J = G for linear-elastic fracture mechanics (LEFM), the J-integral can be used to calculate K for linear-elastic plane strain or plane stress problems. The J-values were calculated for the double-edge crack panel (plane strain) loaded in tension (Fig. 2.9). Three different near-tip mesh configurations were used [Fig. 2.9(a), (b), and (c)], each of which models the $1/\sqrt{r}$ and $\sqrt{r}$ variations in stresses and displacements, respectively, near the crack tip by placing the midside node at the quarter point.[9] The triangular near-tip elements shown in mesh configurations Figs. 2.9(b) and (c) are actually eight-noded isoparametric quadrilaterals that have been collapsed into degenerate triangles by allowing all three node points on one side to share the same location. Studies reported by Wilkinson et al.[11] indicate that the triangular configurations (b) and (c) are somewhat more accurate than (a), because they are better able to model the circumferential variation of the near-tip displacements. Six different integration paths were taken around the crack tip, and a 3 × 3 integration scheme was used. Table 2.1 gives the J-values for each path for each mesh configuration as well as the plane strain K-value (using J_{ave}) obtained from the relation $J = G = K^2/E\ (1 - \nu^2)$. A handbook value for K is also given.[12]

An elastic-plastic J-integral calculation is presently being performed for a compact tension specimen using a near-tip mesh configuration similar to Fig. 2.9(c). Computed J estimates will be compared with an empirical formula derived by Merkle and Corten for this specimen.[13]

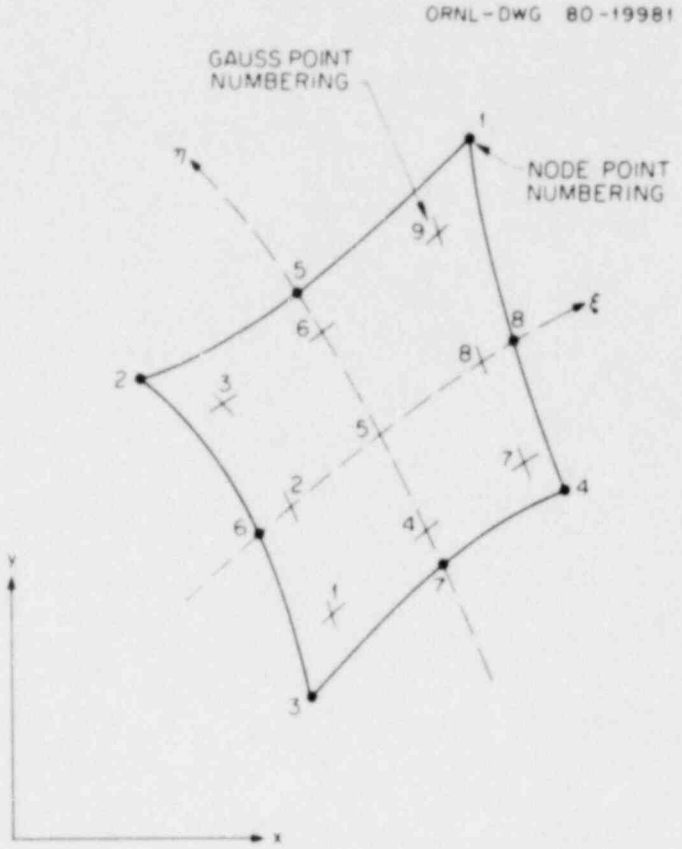

Fig. 2.7. Eight-noded isoparametric element.

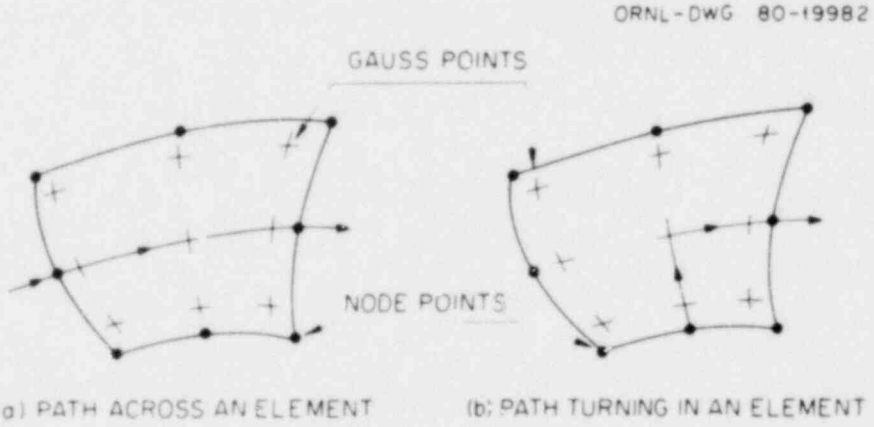

Fig. 2.8. J-integral paths within an element for a 3 × 3 integration scheme.

Table 2.1. Double-edge crack panel in tension (plane strain, P = 4.14 MPa, W = 0.203 m)

Near-tip mesh configuration	kJ/m^2							MPa $\sqrt{m}$	
	J_1	J_2	J_3	J_4	J_5	J_6	J_{ave}	$K = \sqrt{\frac{J_{ave} E}{(1 - \nu^2)}}$	$K_{handbook}$ (Ref. 12)
Fig. 2.9(a)	0.03261	0.03268	0.03270	0.03268	0.03264	0.03266	0.03266	2.725	2.766
Fig. 2.9(b)	0.03271	0.03278	0.03282	0.03280	0.03277	0.03278	0.03278	2.730	2.766
Fig. 2.9(c)	0.03305	0.03280	0.03282	0.03280	0.03277	0.03278	0.03284	2.732	2.766

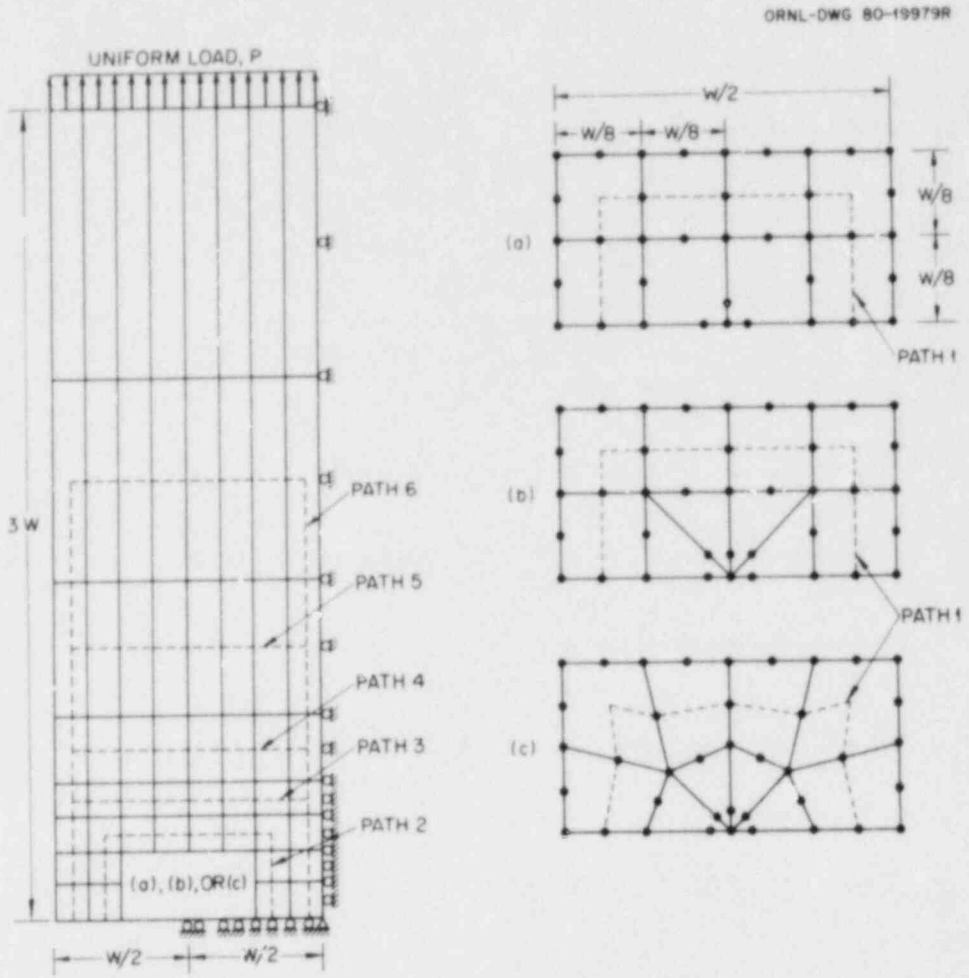

Fig. 2.9. Double-edge crack panel loaded in tension (plane strain, P = 4.14 MPa, W = 203 mm).

2.4 Investigation of Damping and of Cleavage-Fibrous Transition in Reactor-Grade Steel*

W. L. Fourney†

2.4.1 Introduction

The aim of the research program is to investigate in detail the transition region from cleavage to fibrous fracture and its effect on toughness determinations. A complete understanding of this phenomenon is extremely important in predicting fast fracture behavior in a structure.

*Work sponsored by HSST Program under UCCND Subcontract 7778 between Union Carbide Corporation Nuclear Division and the University of Maryland.

†Department of Mechanical Engineering, University of Maryland, College Park, MD 20742.

Within the upper area of the transition temperature range, it is possible to observe onset of rapid cleavage fracturing caused by increases of strain rate at a point of tearing instability. Likewise, in the lower portion of the transition range, sudden fracture of regions of local weakness may cause a conversion from slow fibrous tearing to rapid cleavage prior to the instability point (as estimated in terms of R-curve considerations).

Studies of run-arrest fracturing in crack-arrest specimens have shown that tough, late-breaking regions, which contribute to the diffuse nature of the crack front, occur to a greater degree with increasing toughness and test temperature. Plausible ways exist in which behaviors of this kind can eliminate conditions necessary for dominant cleavage fracturing. Thus, information from crack-arrest research is related to cleavage-fibrous transition research in a natural way.

The expected flaw-probability influence on scatter of toughness values in the lower regions of the transition temperature range, conditions governing onset of cleavage in higher regions of the transition temperature range, and the determination of a temperature T_A high enough to exclude dominant cleavage fracturing are important aspects of transition behavior and are expected results from our research program.

The general topic of cleavage-fibrous transition is complex and difficult, but the importance of advancing understanding in this area is widely recognized. Our research at Maryland will also attract the attention of other research groups and involve them in cleavage-fibrous transition studies.

2.4.2 Research program

To obtain measurement data and a reasonable understanding of the aspects of cleavage-fibrous transition that are of main importance, the following tasks make up the University of Maryland research program during 1980–1981:

A. tearing instability fracture-toughness experiments,
B. investigation of statistical aspects of slow and rapid K_{IC} toughness values,
C. development of a mechanistic model for cleavage-fibrous behavior, and
D. coordination of related work performed at other interested laboratories.

Task A

The purpose of Task A would be to (1) collect information illustrative of the role of tearing instability in causing the onset of dominant cleavage fracturing in the upper portion of the transition temperature range and (2) explore the loss of tearing instability control with reduction of testing temperature. Much of the information needed can be obtained through attracted interest at other laboratories or from samples previously tested elsewhere; however, some testing will be conducted at Maryland. Tests to be conducted for a selected material would include

1. notch bend tests to determine the temperature T_A high enough to exclude dominant cleavage fracturing;
2. 1-T compact tests within the upper region of the transition range to establish the J-R curve for the material chosen;
3. 1-T and 2-T compact tests within the transition range to obtain cleavage fracture inducted by J-R instability; and
4. 1-T and 2-T compact tests at lower temperature to demonstrate loss of J-R-controlled instability.

Task B

Under Task B we propose to

1. collect data from other laboratories that would be pertinent to our study; this would include revieving previous studies of K_{IC} variations (Westinghouse, Alcoa, NASA-Lewis, and others); and
2. use data from Task A to measure test result scatter at a selected temperature.

Our work will be conducted in the most efficient manner, taking account of such data and information as can be obtained from closely related research at other laboratories. Modifications of the test program, as necessary and appropriate, may occur.

Task C

Model development for the transition behavior would involve both photoelastic tests (with polymeric models and birefringent-coated steel samples) as well as 2-D dynamic calculations. Researchers would

1. continue development and refinement of a theoretical model to describe the fibrous-cleavage transition, taking into account weak region (statistical) variations and quenching of cleavage by an increase in late-breaking ligaments;
2. continue trials of computer models of late-breaking ligaments, exploring the effects of locally weak or tough regions;
3. explore photoelastically the effect of local regions of tough or weak material in a specimen and the effect of nonuniform crack fronts on crack advance; and
4. obtain estimates of the closing forces caused by late breaking ligaments using fractography and photoelastic coatings on steel specimens.

Task D

The cleavage-fibrous transition has been of interest to fracture researchers for a very long time. Recent findings suggest that a substantial advance in understanding, particularly of significant practical aspects, is possible. To proceed efficiently toward realization of these

possibilities, the University of Maryland project intends to provide (1) enough examples of clarification to attract wider interest in similar work and (2) coordination and information exchange between those laboratories that are engaged in a cleavage-fibrous research effort. Task D is devoted to coordination and information exchange relative to enhanced understanding of cleavage-fibrous transition behaviors with particular emphasis on aspects of current practical importance to the Nuclear Regulatory Commission (NRC).

2.4.3 Progress to date

Ductile-brittle transition studies

Assistance has been given to an investigation of the fibrous-cleavage transition by thickness reduction measurement and fractographic [stereo viewing — optical and scanning electron microscope (SEM)] examinations of fractured specimens. During this quarter, measurements of the thickness variation along the crack path for both A533B compact samples [tested and supplied by Naval Ship Research and Development Center (NSRDC), Annapolis, Maryland] and A36 three-point bend samples (tested and supplied by Del Research Corporation) have been completed. These results are currently being analyzed.

Fracture-surface topology characterization is being conducted with a parallax bar in stereomicroscopy. Two pairs of stereophotographs of the crack-initiation area were produced at the same regions from the top and bottom fracture surfaces (Fig. 2.10). The specimen selected was an A533B compact tension specimen tested at 59°C. The objectives are not only to determine the opening stretch to correlate with the thickness change measurement, but also to characterize the spread of fracture process zone from the surface roughness. Preliminary measurement of the surface profiles corresponding to Fig. 2.10(a) is shown in Fig. 2.11. Characterization of the other surface is still in progress. Similar measurements will be made from specimens tested at other temperatures. Additionally, specimens in the region where crack arrest occurred will be examined in a similar fashion.

To understand the observed ductile-brittle transition in the three-point bend specimens tested at the Del Research Corporation and to correlate it with other test conditions, standard Charpy V-notch (CVN) impact specimens were machined from some of the three-point bend specimens supplied by Del Research. The specimens were aligned so that the crack path in the CVN specimens was in the same direction as it was in the three-point bend specimens. The specimens tested were primarily in the transition region. The highest temperature at which cleavage was produced during spring-in-series tests of large specimens at Del Research was 66°C. Cleavage did not occur at 79°C, and there were no tests between these two temperatures. Results of the CVN energy vs temperature tests are shown in Fig. 2.12. Fracture surface observation indicated that at 60°C fracture initiated in ductile-fibrous mode, but islands of cleavage failures appeared in the midsection of the specimen. The amount of cleavage islands found in the specimen tested at 80°C was much less than that at 60°C and

ORNL–PHOTO 0540–81

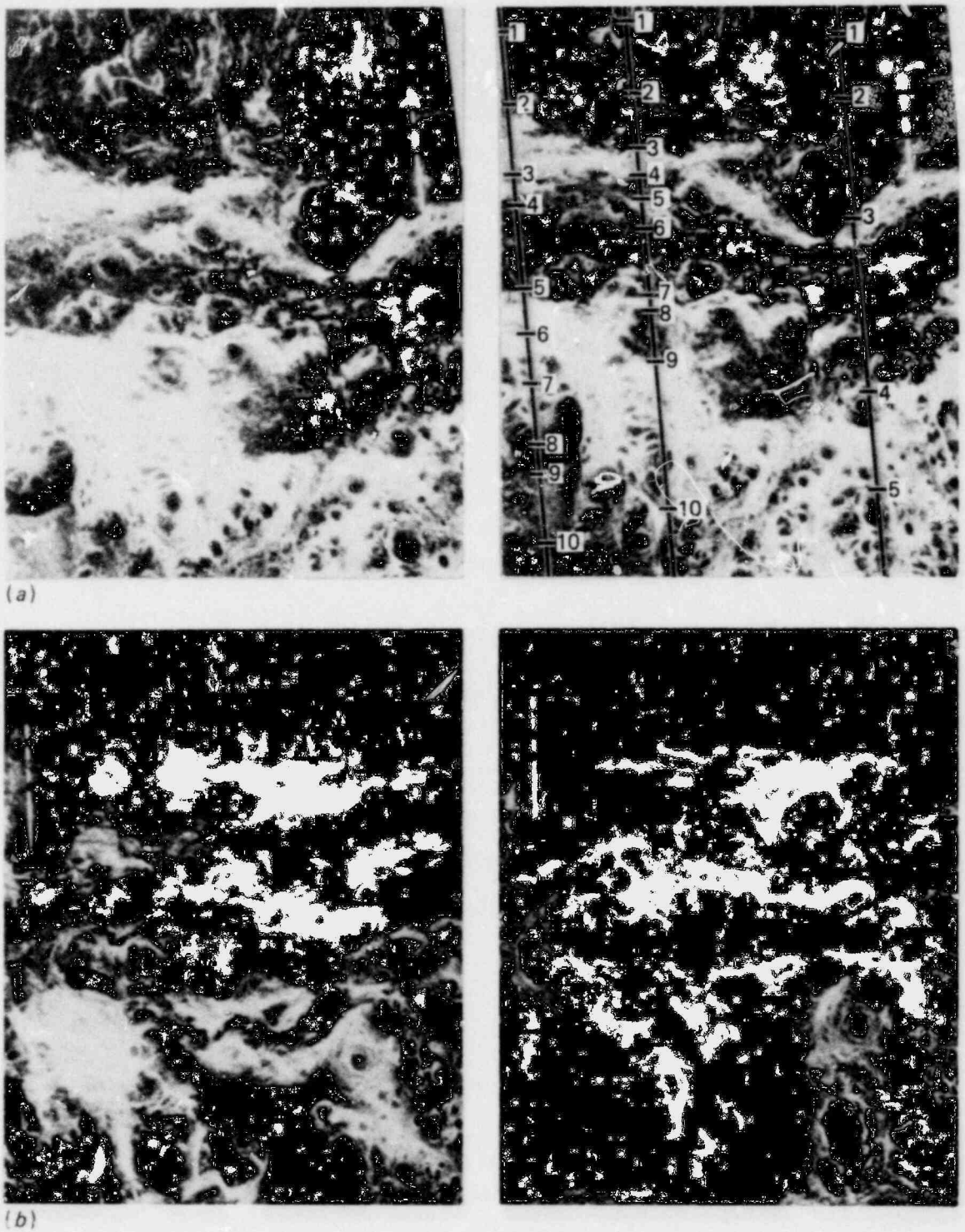

Fig. 2.10. SEM stereomicrographs showing (a) crack initiation region on top fracture surface and (b) matching area on bottom surface. Lines a, b, and c are for height measurement locations shown in Fig. 2.11.

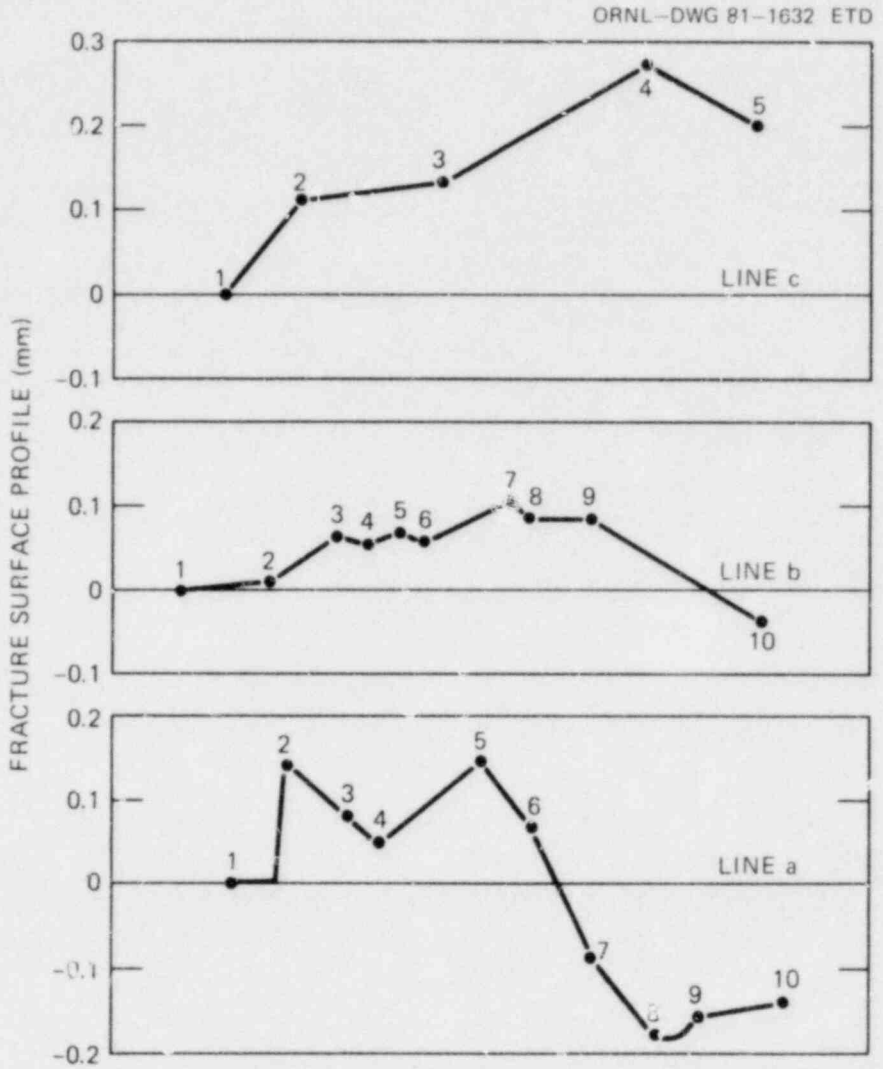

Fig. 2.11. Fracture surface profile along lines shown in Fig. 2.10(a).

could almost be considered nonexistent. The specimen tested at 100°C did not show any sign of cleavage fracture. Based on the observation of fracture surfaces, the upper-limit temperature for the occurrence of cleavage fracture is considered to be about 80°C. This observation appears to be in agreement with the one made from the three-point bend specimen tested with a spring plate in the loading system. Although this result is presently for only one steel material, the result suggests that normal Charpy testing may provide a convenient indication of the highest temperature at which cleavage can occur during stable fibrous crack extension in a service component.

A similar comparison will be soon available for the A533B steel tested at the David Taylor Naval Ship Research and Development Center (NSRDC) at Annapolis. In addition, because of interest generated in

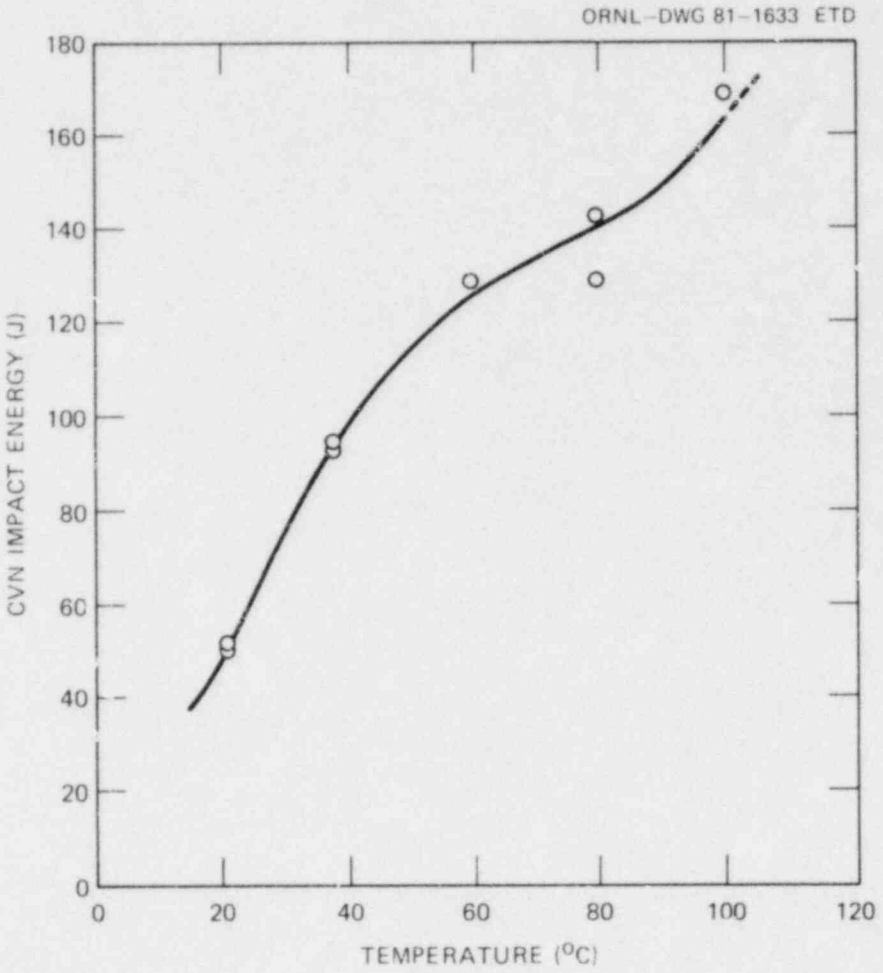

Fig. 2.12. CVN impact energy as function of temperature for A36 steel.

transition range testing at other organizations, similar results will eventually be available for five different steels or heat treatments of the same steel.

Photoelastic investigations

Introduction. The described results are directed toward (1) improving existing techniques for determination of K from photoelastic fracture patterns, (2) determining the variation with crack-tip position of the nonsingular terms associated with several different fracture test specimens, and (3) characterizing and quantifying the size of the singularity-dominated zone in these specimens.

As established previously,[14-16] accurate determinations of K frequently require the use of nonsingular terms, and techniques have been developed to determine the required number of parameters from isochromatic

crack-tip fringe patterns.[16,17] Part of the current year's research program consists of developing a mechanistic model for the cleavage-fibrous transition observed in steels. Photoelastic experiments are planned in which the effects on K of locally tough or weak regions of material will be studied, and the effects of diffused crack fronts will also be investigated. A meaningful analysis of data from these studies required the determination of K to a high degree of accuracy, and consequently, a need exists for understanding the behavior of nonsingular terms that are required for an adequate stress field representation.

The stress field representation used is based on the Airy Stress Function for a static stress field involving a single crack tip. If the coordinate origin is located at the crack tip and the negative x-axis coincides with the crack faces, the stress function may then be written as:[14,15]

$$F = \mathrm{Re}\,\bar{\bar{Z}} + y\,\mathrm{Im}\,(\bar{Z} + \bar{Y}) \,, \tag{1}$$

where

$$Z(z) = \sum_{n=o}^{n=N} A_n\, z^{n-(1/2)} \,, \tag{2}$$

$$Y(z) = \sum_{m=o}^{m=M} B_m z^m \,, \tag{3}$$

$$z = x + iy \,, \tag{4}$$

$$Z = \frac{d\bar{Z}}{dz} \,, \tag{5}$$

$$\bar{Z} = \frac{d\bar{\bar{Z}}}{dz} \,, \tag{6}$$

$$Y = \frac{d\bar{Y}}{dz} \,, \tag{7}$$

and the A_n and B_m are real constants.

In the following paragraphs, results are presented for the nonsingular term variation in modified-compact tension (MCT) and rectangular-double-cantilever-beam (RDCB) specimens. In addition, preliminary results are presented for the singularity-dominated zone size in these specimens.

Nonsingular term variation in MCT and RDCB specimens. The MCT specimens of standard geometry[18] and two different size (w_S = 101.6 mm and w_L = 203.2 mm) were used for the first part of the study. The specimen geometry and the loading were as shown in Fig. 2.13. Isochromatic fringe patterns were recorded at several different crack lengths and load levels in the two different size specimens, and the results were used to establish the form of Eqs. (2) and (3) that are independent of the load and specimen size. The modified form of these equations was determined to be:[19]

$$Z(z) = \frac{K}{\sqrt{2\pi w}} (z/w)^{-(1/2)} \sum_{n=o}^{n=N} A_n' (z/w)^n , \qquad (8)$$

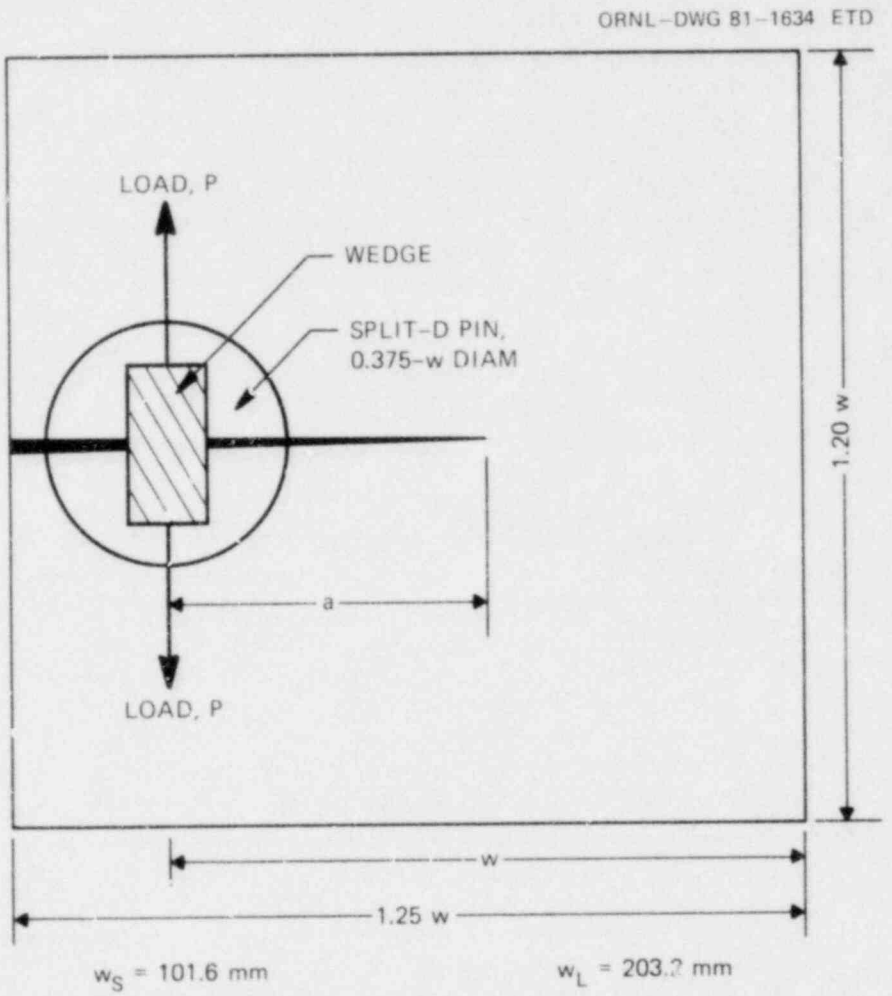

Fig. 2.13. Geometry and loading of modified-compact-tension (MCT) specimen.

and

$$Y(z) = \frac{K}{\sqrt{2\pi w}} (z/w)^{-(1/2)} \sum_{m=o}^{m=M} B'_m (z/w)^{m+(1/2)} , \qquad (9)$$

where w is a characteristic in-plane dimension of the specimen, such as the specimen width.

The variation with crack position of the isochromatic fringe patterns in an MCT specimen is illustrated in Fig. 2.14. Data points were taken over a circular region of radius 0.125w (marked on each photograph in Fig. 2.14) and analyzed using a multiple-point, nonlinear, least-squares method[16,17] to obtain the first eight coefficients of the series representation (A'_0 to A'_3 and B'_0 to B'_3).

As the number of coefficients increased from two to eight, Fig. 2.15 shows the change in the average fringe order error between observed and calculated fringe orders. In each case, the error term stabilizes by the time the eighth coefficient is added, indicating that the stress field has been adequately modeled over the region of data acquisition.

The variation with a/w of the first six coefficients is shown in Fig. 2.16. Notice the strong influence of the approaching normal boundary that is manifested in the dramatic increase of the nonsingular coefficients from a/w = 0.70 to a/w = 0.90. From these results, it can be anticipated that the size of the singularity-dominated zone will show a sharp decrease as the boundary is approached.

A wedge-loaded RDCB specimen (with w = 279 mm) was used for the second part of the study. The geometry and loading are shown in Fig. 2.17, and the choice of this specimen was based on a desire to investigate a specimen whose anticipated behavior was substantially different from that of an MCT specimen. The fringe pattern variation with crack length observed in the RDCB specimen is illustrated in Fig. 2.18. Once again, the circle indicated on each photograph is the region over which data were acquired for analysis. In this case, the radius of the circle is 0.091w. Figure 2.19 shows the change in average fringe order error that was experienced for this specimen, and once again, stabilization of the error term was observed to occur by the time eight coefficients were used.

The first six coefficients of an eight-parameter solution are shown as functions of a/w in Fig. 2.20. With the exception B'_0, all the nonsingular terms remained essentially constant over the entire range from a/w = 0.30 to a/w = 0.70, after which they begin to change dramatically. The behavior of B'_0 is too complicated to discuss in detail here but will be covered in a topical report to appear in February.

These data are consistent with the isochromatic fringe patterns observed (Fig. 2.18) and are also consistent with the geometry of the specimen. Until a/w = 0.75, the specimen boundaries that are closer to the crack tip are the boundaries parallel to the crack line. Because these boundaries remain the same distance from the crack tip over the span a/w = 0.30 to a/w = 0.70, the nonsingular terms (whose presence in the stress field representation is due to the existence of finite specimen boundaries) can also be expected to show only small changes with crack-tip position. Once again, behavior of the nonsingular terms can be used

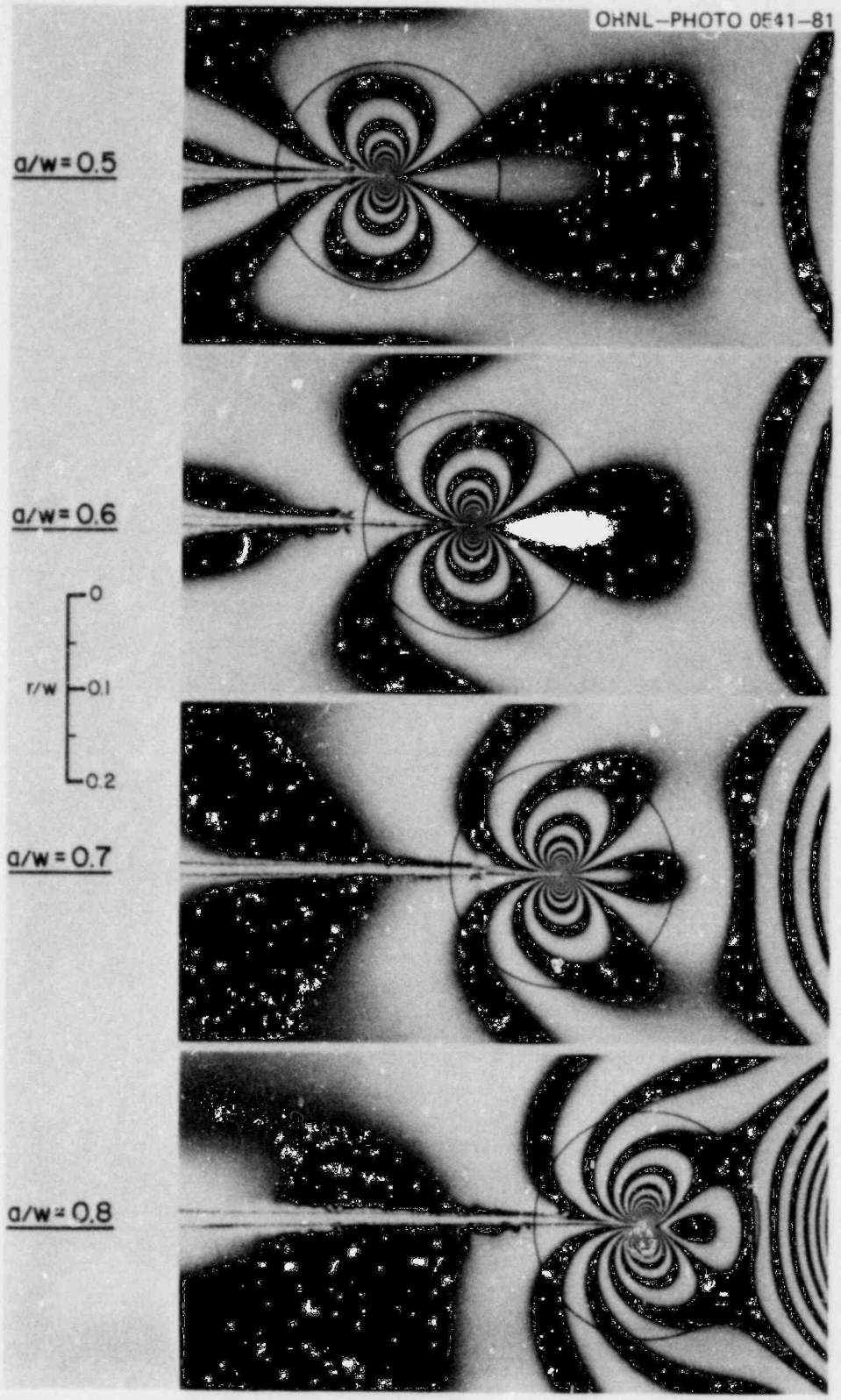

Fig. 2.14. Isochromatic fringe patterns recorded at several different crack lengths in an MCT specimen illustrating changes in fringe patterns as boundary is approached.

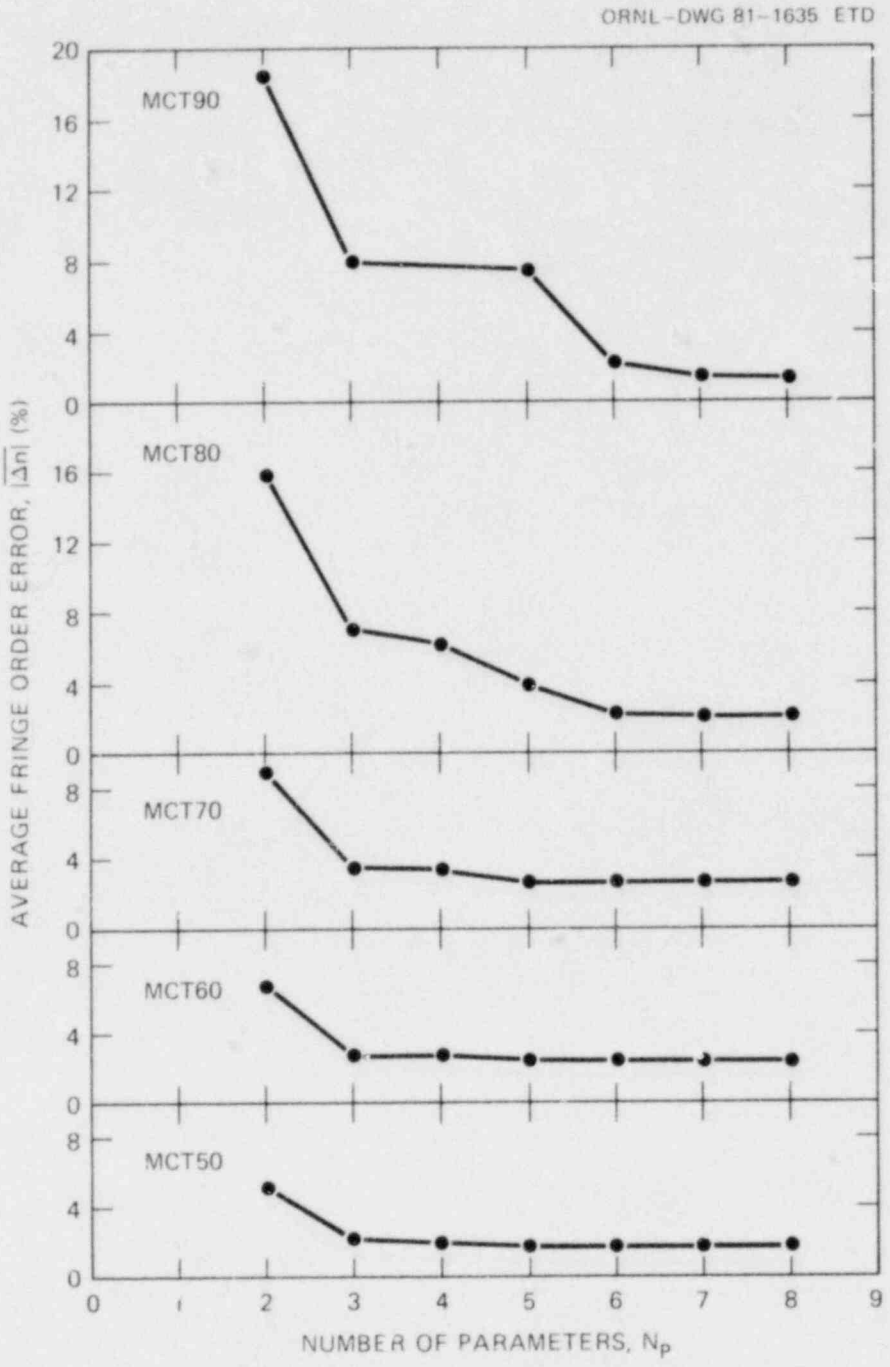

Fig. 2.15. Average fringe order error as function of number of coefficients used in series stress field representation (MCT specimen).

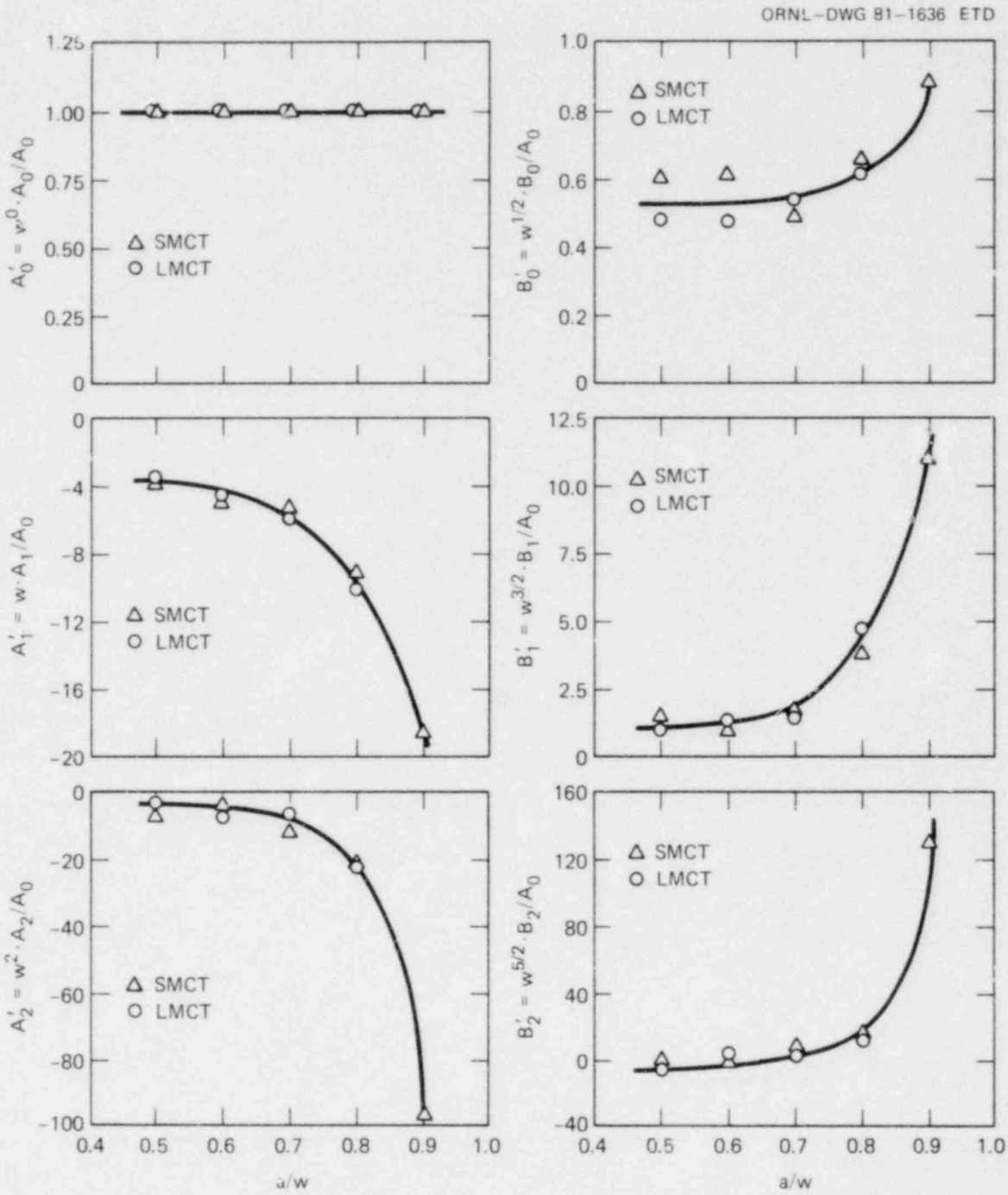

Fig. 2.16. Variation with crack length of first six coefficients in series stress field representation as obtained from two different sizes of MCT specimen.

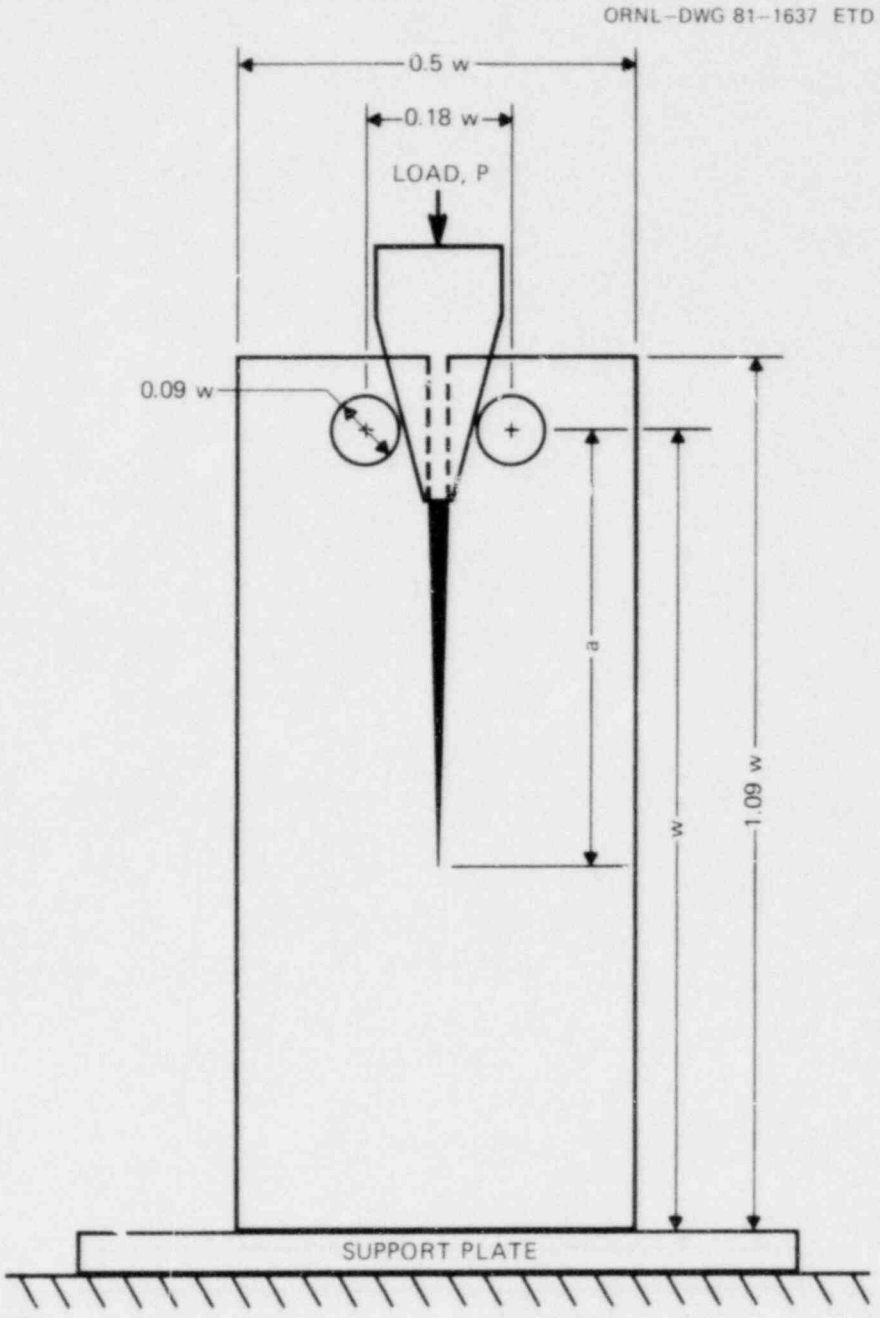

Fig. 2.17. Geometry and loading of wedge-loading RDCB specimen used for this study.

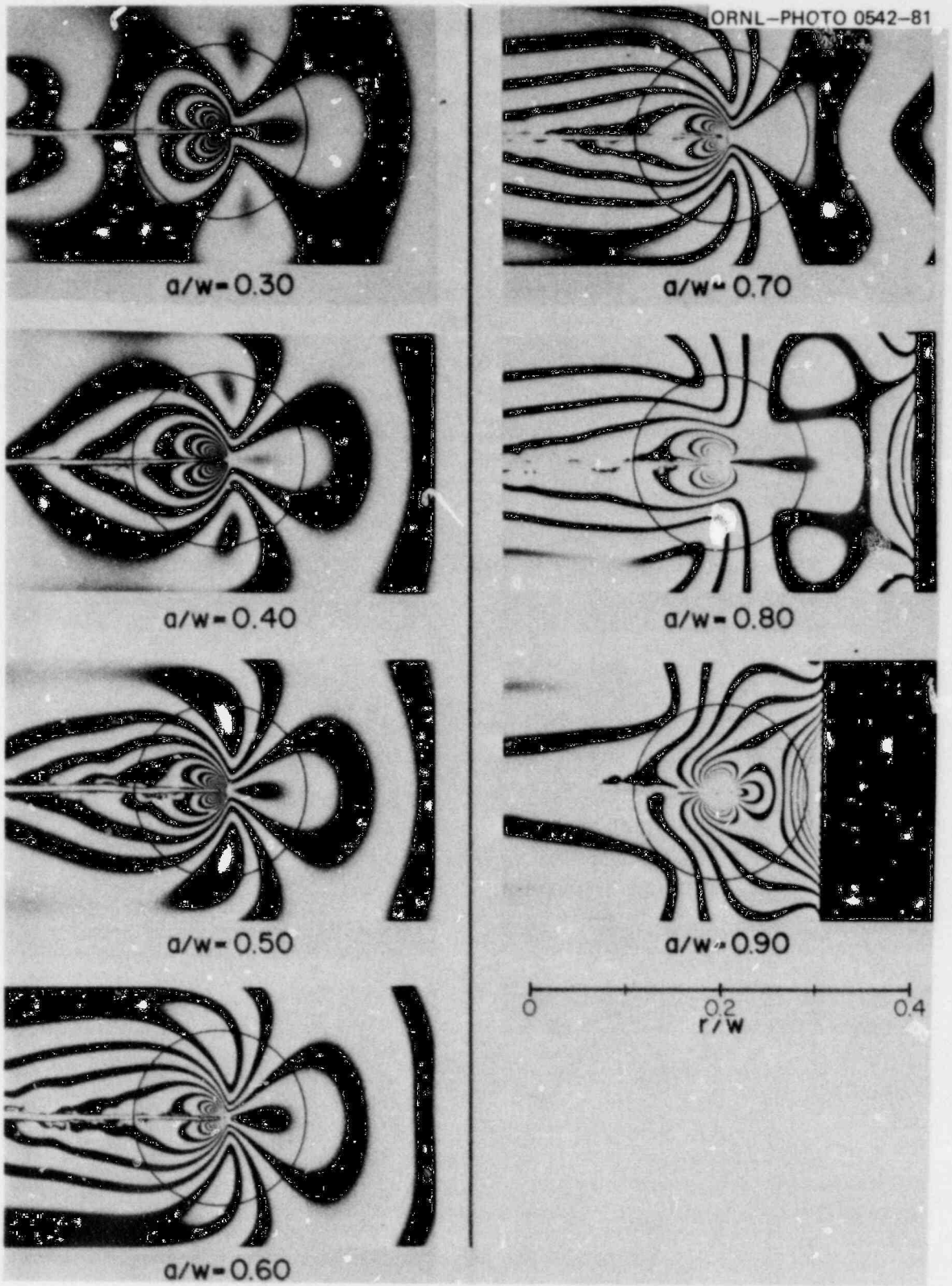

Fig. 2.18. Isochromatic fringe patterns recorded at several different crack lengths in an RDCB specimen illustrating changes in fringe patterns as crack is extended toward boundary.

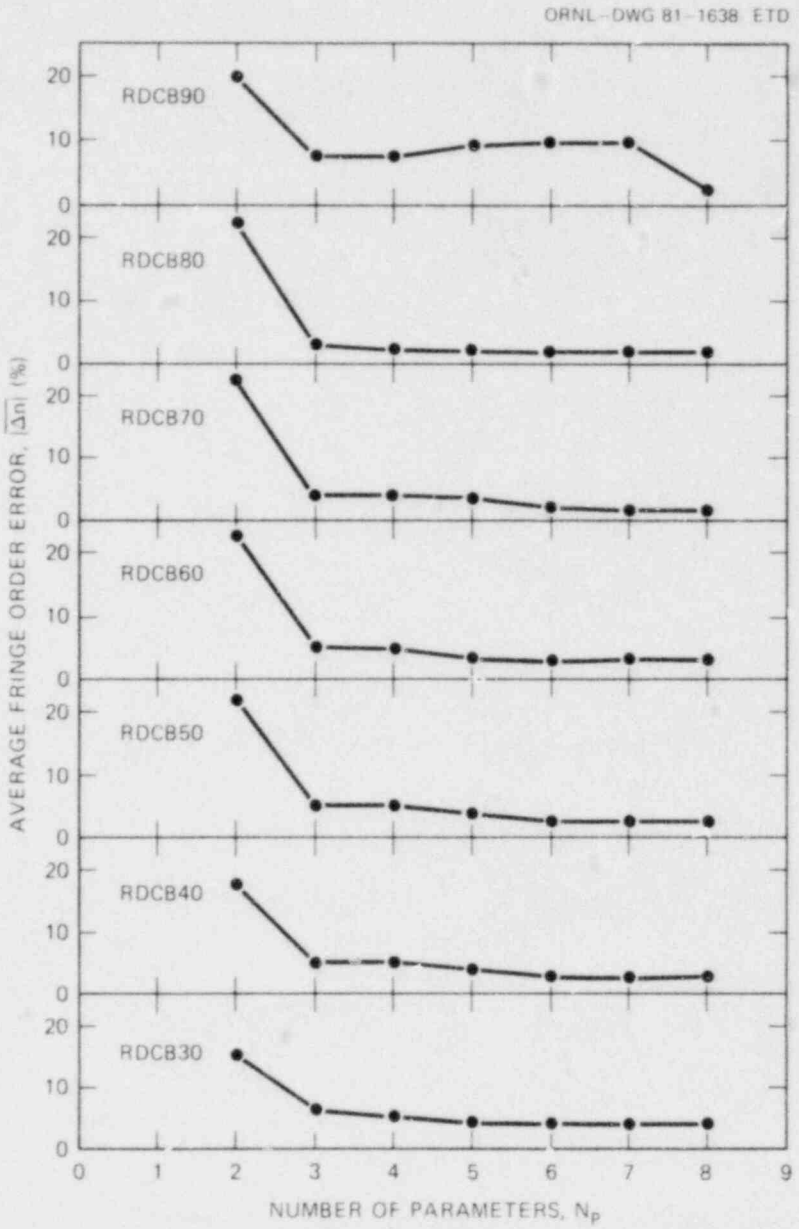

Fig. 2.19. Average fringe order error as function of number of coefficients used in series stress field representation (RDCB specimen).

to anticipate variations in the singularity-dominated zone in the RDCB specimen.

Results for the singularity-dominated zone in MCT and RDCB specimens. Among the various measures for the singularity-dominated zone that have been studied, the crack opening stress σ_y offers the most promise. For example, Fig. 2.21 shows the regions surrounding the crack tip (at a/w = 0.60 in an MCT specimen) in which σ_x, σ_y, and τ_{xy} from six-parameter and

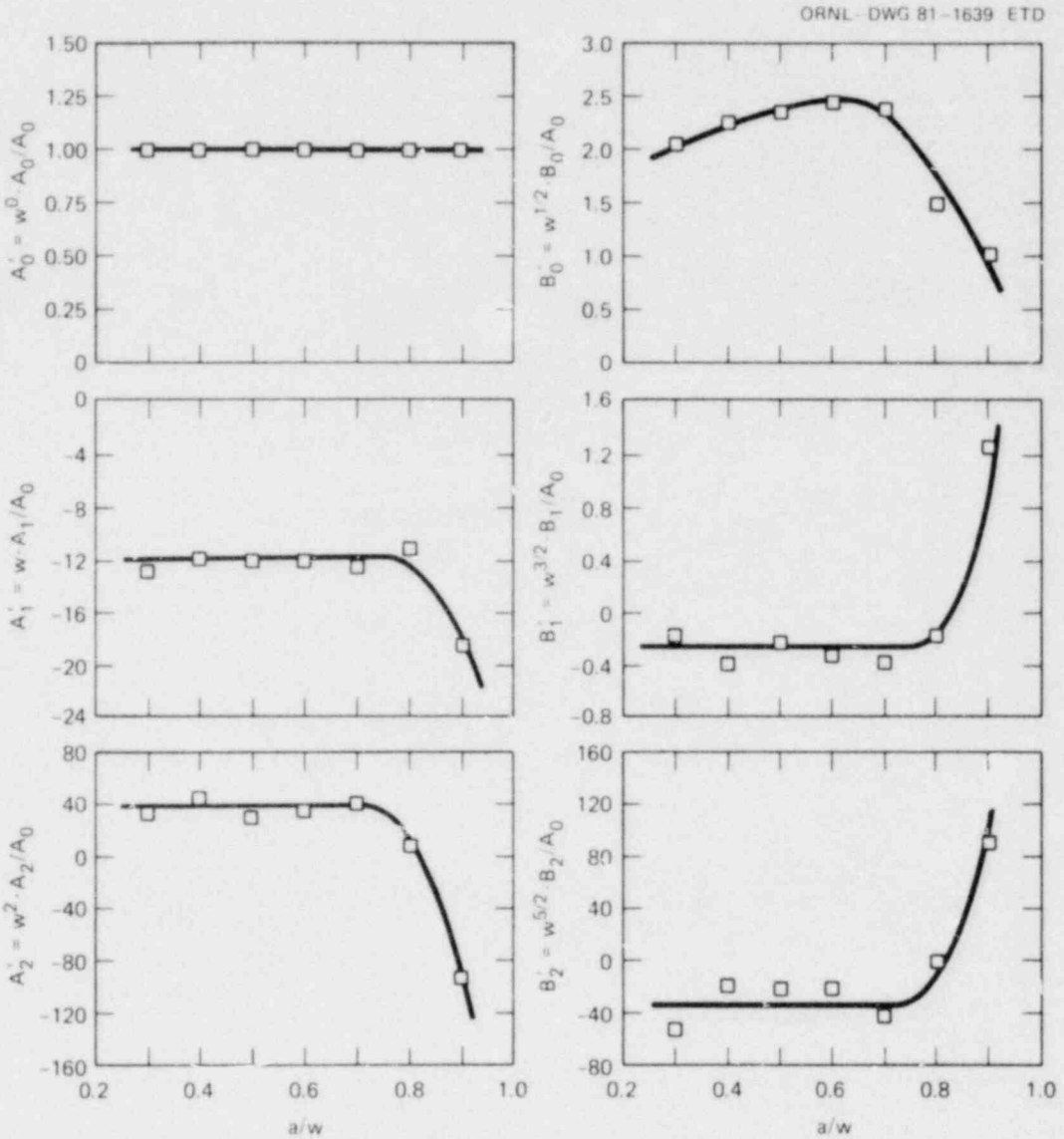

Fig. 2.20. Variation with crack length of first six coefficients in series stress field representation as obtained for RDCB specimen.

singular solutions differ by <2%. Clearly, only the region based on a 2% error in σ_y can qualify for the title of a "zone."

A series of similar zones has been obtained for both the MCT and RDCB specimens, using values for the nonsingular terms shown in Figs. 2.16 and 2.20. Shown in Fig. 2.22 are the 2% error zones for σ_y corresponding to several different crack lengths in an MCT specimen. Notice that the minimum radius of the zone, r_{min}, occurs at $\theta = 0°$ in each case. A plot of r_{min}/w as a function of a/w is shown in Fig. 2.23 for both MCT and RDCB specimens. As anticipated from the nonsingular term variation, the zone size in the RDCB specimen remains constant over a large region before

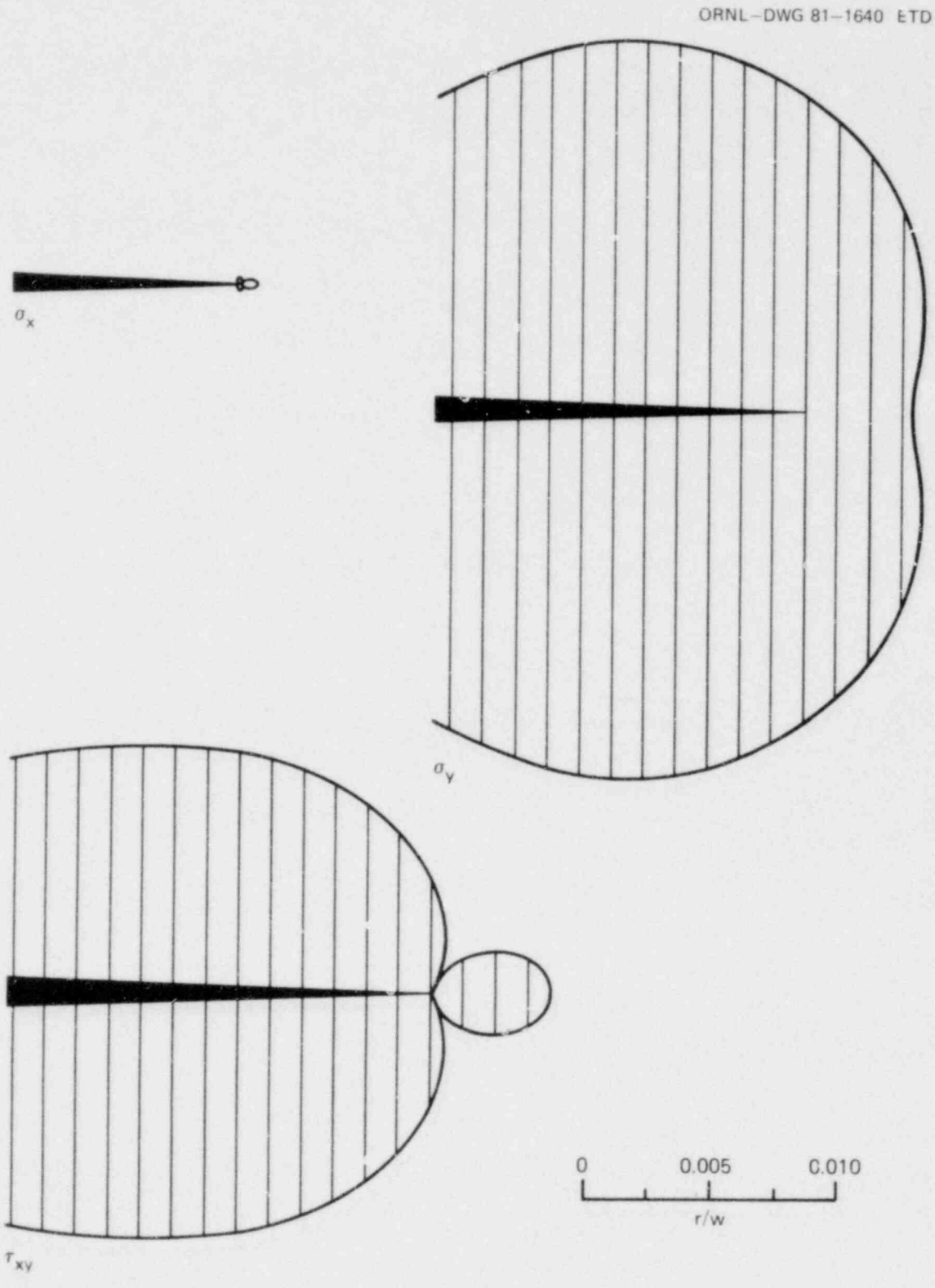

Fig. 2.21. Regions surrounding crack tip at $a/w = 0.6$ in an MCT specimen in which six-parameter and singular solutions for σ_x, σ_y, and τ_{xy} differ by <2%.

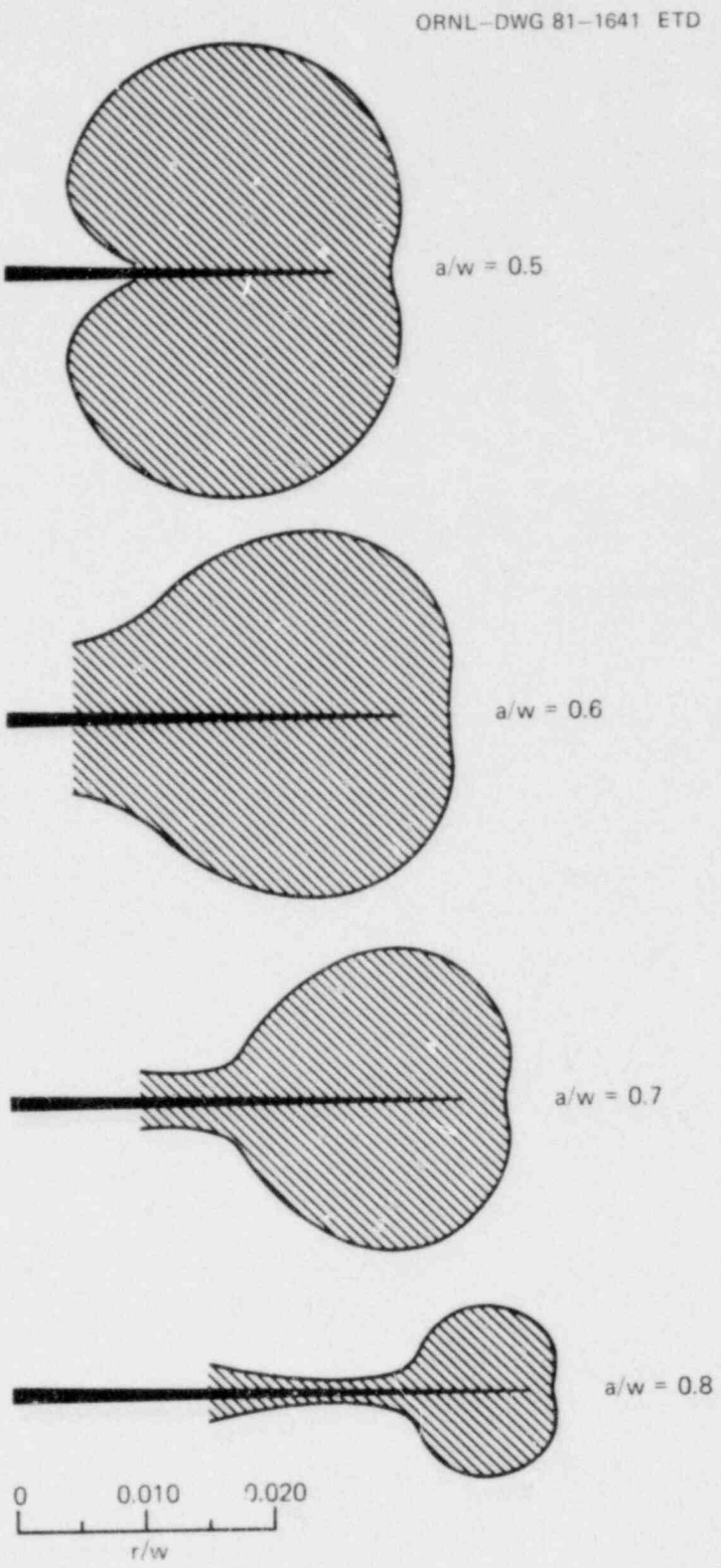

Fig. 2.22. Changes observed in zone surrounding crack tip at several different crack lengths in an MCT specimen for which six-parameter and singular solutions for σ_y differ by <2%.

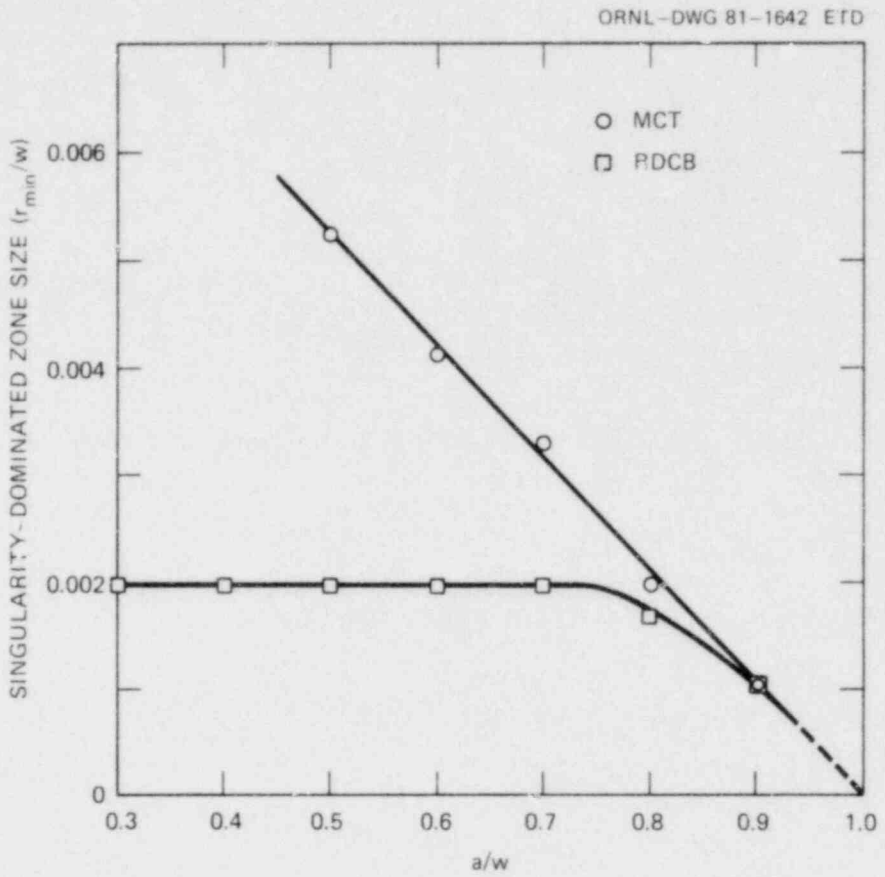

Fig. 2.23. Variation with a/w of the singularity-dominated zone size in MCT and RDCB specimens.

starting to decrease sharply, whereas the zone size in the MCT specimen displays a steady decrease over the region studied. Note that the span from a/w = 0.30 to a/w = 0.90, which has been investigated in the MCT specimen, always has the boundary normal to the crack line as the nearest boundary. In contrast, the region of investigation in the RDCB specimen (a/w = 0.20 to a/w = 0.90) is predominantly influenced by the parallel boundaries, as discussed earlier.

An examination of the zone size as a function of the distance to nearest boundary R_{min} provides some interesting results. Shown in Fig. 2.24, as functions of a/w, are r_{min}/R_{min} for the RDCB specimen and $r_{min}/(w - a)$ for the MCT and RDCB specimens, where $w - a$ is the net remaining ligament ahead of the crack tip. In the case of the MCT specimen, r_{min} is observed to be a constant percentage of the net ligament, with the 2% error zone in σ_y providing a value of r_{min} equal to 1% of $(w - a)$.

A similar plot for the RDCB specimen shows rather different behavior. A plot r_{min}/R_{min} for the RDCB specimen is much easier to interpret. Over the range from a/w = 0.30 to a/w = 0.70, both r_{min} and R_{min} are constants, and their ratio also remains constant. At and beyond a/w = 0.75, the behavior of r_{min}/R_{min} becomes the same as that of $r_{min}/(w - a)$; beyond an a/w of 0.90, the approaching normal boundary dominates to such an extent

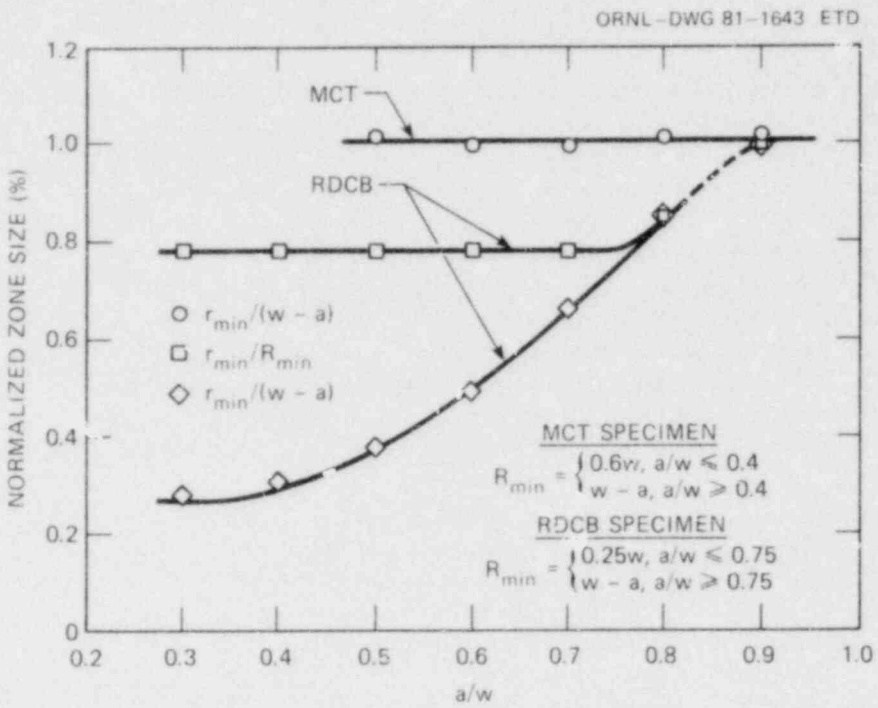

Fig. 2.24. Singularity-dominated zone size in MCT and RDCB specimens as related to net ligament ahead of crack and distance to nearest specimen boundary.

that the behavior of both RDCB and MCT specimens is essentially the same. Indications of this can be obtained from an examination of the RDCB fringe pattern at a/w = 0.90, which shows features similar to those observed for long cracks in MCT specimens. This behavior is also evident from the nonsingular terms, which in magnitude and sign approach the values obtained for the MCT specimen.

The most important result to be noted here is that, over much of the span of the specimen, the singularity-dominated zone size in an MCT specimen is substantially larger than that in an RDCB specimen of the same width.

Conclusions. Based on the results to date, these conclusions are possible:

1. the nonsingular terms in the series stress field representation are specimen-size independent;
2. for a given specimen geometry, the nonsingular terms display a systematic variation with crack length;
3. significant differences exist in the size of the singularity-dominated zone between various fracture test specimens;
4. within any one specimen type, the size of the singularity-dominated zone varies with crack length; and
5. the absolute size of the singularity-dominated zone is specimen-size dependent.

2.4.4 Interaction with other organizations

Interest in cleavage-fibrous transition studies continues at Picatinni Arsenal. In December, Picatinni Arsenal obtained a supply of 2-in.-thick A514 steel plate material at Fritz Laboratory, Lehigh University. Test specimens will be made from this material and a repetition of previous testing with A36 steel will be conducted.

During this past quarter, ORNL reviewed the current results of cleavage-fibrous transition studies at the University of Maryland. An extension of the comparisons with as-quenched A533B material was discussed and might possibly be conducted at ORNL.

The NSRDC scheduled additional testing with steels that have particular interest to the Navy. In particular, they plan on testing the two steels HY80 and HY130. The NSRDC expects to compare the test temperature at which the disappearance of cleavage fracture occurs in CVN specimens and in large compact specimens tested with a spring in series.

Testing at the various organizations mentioned, therefore, will include five different steels: A533B, A36, A514, HY80, and HY130 (and two different heat treatments of A533B).

A limited size seminar covering various aspects of cleavage-fibrous transition research is planned for late January at Maryland University. The purpose of this meeting is to review progress and establish sensible goals — not only for the research being conducted at the University of Maryland, but for the overall program.

References

1. J. W. Bryson and B. R. Bass, "A Computer Program (NOZ-FLAW) for Direct Evaluation of K-Factors for Arbitrarily Shaped Flaws at Pressure Vessel Nozzle Corners," *Heavy-Section Steel Technology Program Quart. Prog. Rep. July–September 1980*, NUREG/CR-1806 (ORNL/NUREG/TM-419), pp. 3–9.

2. B. R. Bass, J. W. Bryson, and K. Kathiresan, *NOZ-FLAW: A Finite Element Program for Direct Evaluation of Stress Intensity Factors for Pressure-Vessel Nozzle Corner Flaws*, ORNL/NUREG/CSD/TM-18 (to be published).

3. B. R. Bass, J. W. Bryson, and K. Kathiresan, *OR-FLAW: A Finite Element Program for Direct Evaluation of K-Factors for User Defined Flaws in Plates, Cylinders, and Pressure-Vessel Nozzle Corners* (to be published).

4. K. J. Bathe, *ADINAT — A Finite Element Program for Automatic Dynamic Incremental Nonlinear Analysis of Temperatures*, Report 82448-5, Mechanical Engineering Department, Massachusetts Institute of Technology (May 1977).

5. J. W. Bryson, B. R. Bass, and R. H. Bryan, "Determination of K-Factors for Nozzle-Corner Flaws Under Combined Pressure-Thermal Loading," *Heavy-Section Steel Technology Program Quart. Prog. Rep. April–June 1980*, NUREG/CR-1627 (ORNL/NUREG/TM-401), pp. 3-5.

6. K. J. Bathe, *ADINA — A Finite Element Program for Automatic Dynamic Incremental Nonlinear Analysis*, Report 82448-1, Mechanical Engineering Department, Massachusetts Institute of Technology (May 1977).

7. P. M. Besuner, D. C. Peters, and R. C. Cipolla, *BIGIF: Fracture Mechanics Code for Structures*, NP-838, Failure Analysis Associates (July 1978).

8. R. H. Bryan et al., *Test of 6-in.-thick Pressure Vessels Series 3: Intermediate Test Vessel V-8*, ORNL/NUREG-58, pp. 128–130 (December 1979).

9. R. D. Henshell and K. G. Shaw, "Crack Tip Finite Elements Are Unnecessary," *Int. J. Numer. Methods Eng.* 9, 495–507 (1975).

10. H. G. deLorenzi, *J-Integral and Crack Growth Calculations with the Finite Element Program ADINA*, Corporate Research and Development, General Electric Company, Schenectady, New York, August 15, 1978.

11. J. P. D. Wilkinson et al., *Methodology for Plastic Fracture — First Quarterly Report, February 16 to July 31, 1976*, Corporate Research and Development, General Electric Company, Schenectady, New York (July 1976).

12. J. F. Knott, *Fundamentals of Fracture Mechanics*, Halsted Press, John Wiley and Sons, New York, 1973.

13. J. G. Merkle and H. T. Corten, "A J-Integral Analysis for the Compact Specimen, Considering Axial Force as Well as Bending Effects," *J. Pressure Vessel Technol.* 96, 286–292 (November 1974).

14. R. J. Sanford, "A Critical Re-examination of the Westergaard Method for Solving Opening-Mode Crack Problems," *Mech. Res. Commun.* 6, 289–294 (1979).

15. R. Chona, G. R. Irwin, and A. Shukla, "A Comparison of Two and Three Parameter Representations of the Stress Field Around Static and Dynamic Cracks," *Exp. Mech.* (to be published).

16. G. R. Irwin et al., "Photoelastic Studies of Damping, Crack Propagation, and Crack Arrest in Polymers and 4340 Steel," NRC Report NUREG/CR-1455 (1979).

17. R. J. Sanford, "Application of the Least Squares Method to Photoelastic Analysis," *Exp. Mech.* 20, 192–197 (1980).

18. ASTM E5o1-80, *Standard Recommended Practice for R-Curve Determination*, Amercian Society for Testing and Materials, Philadelphia, PA, 1980.

19. W. L. Fourney, "Investigation of Damping and of Cle vage-Fibrous Transition in Reactor-Grade Steel," *Heavy-Section Steel Technology Program Quart. Prog. Rep. July–September 1980*, NUREG/CR-1806 (ORNL/NUREG/TM-419), pp. 10–28.

3. INVESTIGATIONS OF IRRADIATED MATERIALS

3.1 Second and Third 4T-CTS Irradiation Studies

D. A. Canonico T. N. Jones
R. G. Berggren

The remainder of the CVN impact specimens from these irradiation experiments were tested. Preliminary examination of the results indicates conformance with those for specimens previously tested.[1,2] Fast load drop and energy-to-maximum load data are being obtained, and all results will be analyzed on the basis of fast neutron fluence and irradiation temperature.

3.2 Fourth HSST Irradiation Series

J. W. Woods T. N. Jones
R. G. Berggren D. A. Canonico

Irradiation of the first capsule, Capsule A, of the irradiation series was completed in October 1980. The capsule was irradiated for 4630 h, and temperature control was excellent during the entire period.

Irradiation of the second capsule, Capsule B, continued through this quarter.

Parts for the third capsule of this series are on hand. The 1T compact specimens have been fatigue precracked; final inspection, including compliance measurements, is in progress.

References

1. R. G. Berggren et al., "Investigations of Irradiated Materials," *Heavy-Section Steel Technology Program Quart. Prog. Rep. July–September 1979*, ORNL/NUREG/TM-370, pp. 27–39.

2. D. A. Canonico et al., "Investigation of Irradiated Materials," *Heavy-Section Steel Technology Program Quart. Prog. Rep. April–June 1980*, ORNL/NUREG/TM-401, pp. 18–27.

4. THERMAL SHOCK INVESTIGATIONS*

R. D. Cheverton S. K. Iskander

During this report period, a preliminary posttest analysis of TSE-5A was completed for the thermal-shock program, and a thermal-fracture-mechanics computer code referred to as OCA (overcooling accident) was written.

4.1 Preliminary Analysis of TSE-5A

The purpose of thermal-shock experiment TSE-5A, which was conducted on September 24, 1980, was to achieve (1) initiation and arrest of shallow and deep flaws, (2) a series of initiation-arrest events, (3) warm prestressing, and (4) arrest in a rising K_I field [$dK_I/d(a/w) = 0$]. Each of these objectives was met. Test conditions for TSE-5A are summarized in Table 4.1, and a set of pretest critical-crack-depth curves, which indicates the expected behavior of the long axial flaw, is presented in Fig. 4.1. The pretest analysis and the technique for conducting the experiment are discussed in Ref. 1.

*Conversions from SI to English units for all SI quantities are listed on a foldout page at the end of this report.

Table 4.1. Test conditions for TSE-5A

Test specimen	TSC-2
Test specimen dimensions, m	
OD	0.991
ID	0.686
Length	1.22
Test specimen material	A508, Class-2 chemistry
Test specimen heat treatment	Tempered at 679°C for 4 h
K_{Ic} and K_{Ia} curves used in design	Lower-bound K_{Ic} and mean K_{Ia} data from ORNL and Battelle Columbus Laboratories TSE-5A material-characterization studies (Fig. 4.8)
Flaw	Long axial sharp crack, a = 11 mm
Temperatures, °C	
Wall (initial)	93
Sink	−100
Coolant	LN_2
Flow conditions	Natural convection
Coating on quenched surface	Rubber cement (3M-NF34)
Coating surface density, g/m^2	270

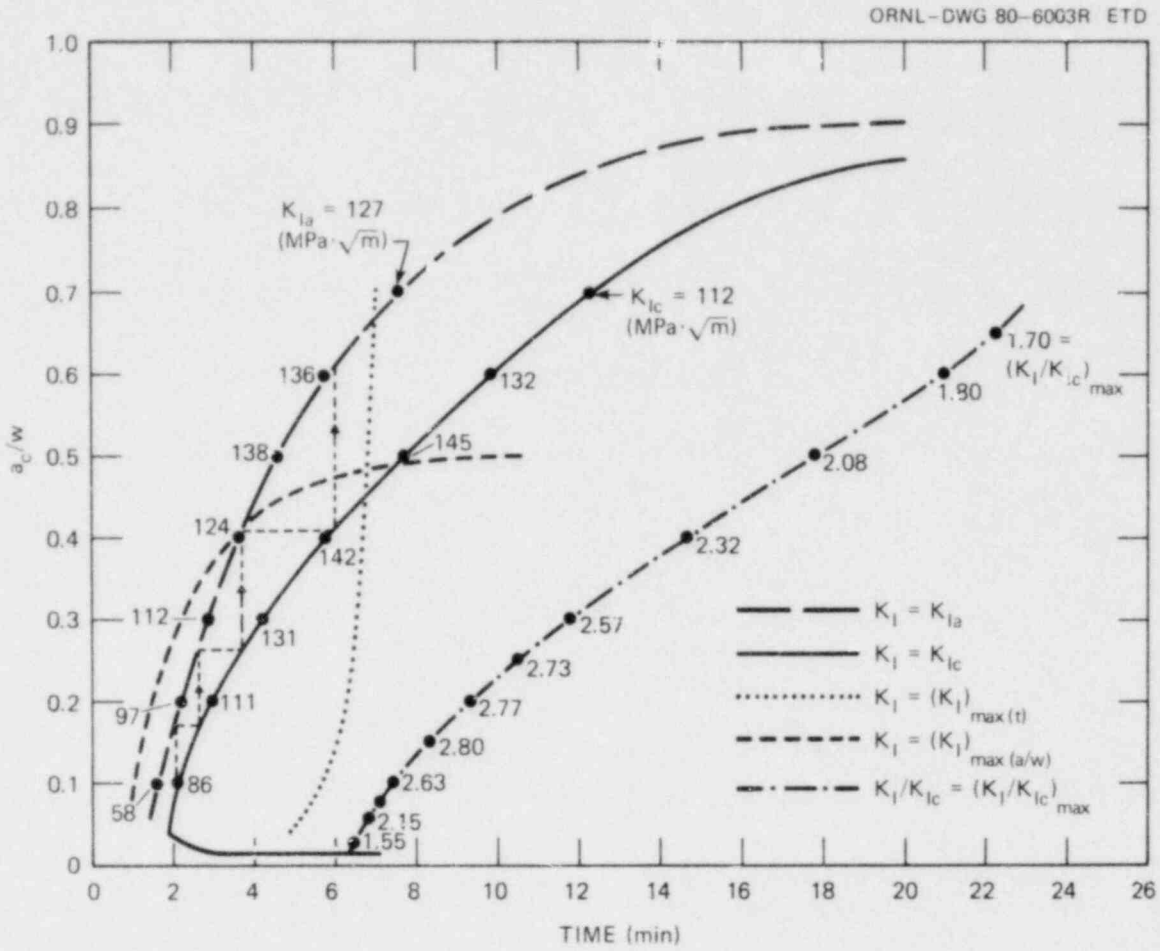

Fig. 4.1. Pretest critical-crack-depth curves for TSE-5A assuming TSE-5 thermal transient and TSE-5A lower-bound K_{Ic} and mean K_{Ia}.

The most significant results of TSE-5A are summarized as follows: (1) warm prestressing of a deep flaw ($a/w \cong 0.5$) was conclusively demonstrated [$(K_I/K_{Ic})_{max} = 2.3$], (2) arrest in a rising K_I field was demonstrated, and (3) the effective fracture and arrest toughnesses of the test cylinder were significantly less than the values derived from the pretest material-characterization studies, corresponding to a temperature shift of approximately +22 K.

The trace of the crack-opening displacement (COD) output (Fig. 4.2) illustrates graphically the initiation-arrest events that took place during TSE-5A. As indicated, major initiation-arrest events took place at 78.5, 90.5, 173.0, and 184.5 s. There were no indications of events after 184.5 s. The corresponding crack depths at arrest near midlength of the test cylinder [as determined with the ultrasonic (UT) instrumentation] were 17, 31, 41, and 81 mm. The full-length crack-depth profiles as determined from UT data are presented in Fig. 4.3, which shows that the cracks are shallower near the ends of the cylinder than elsewhere.

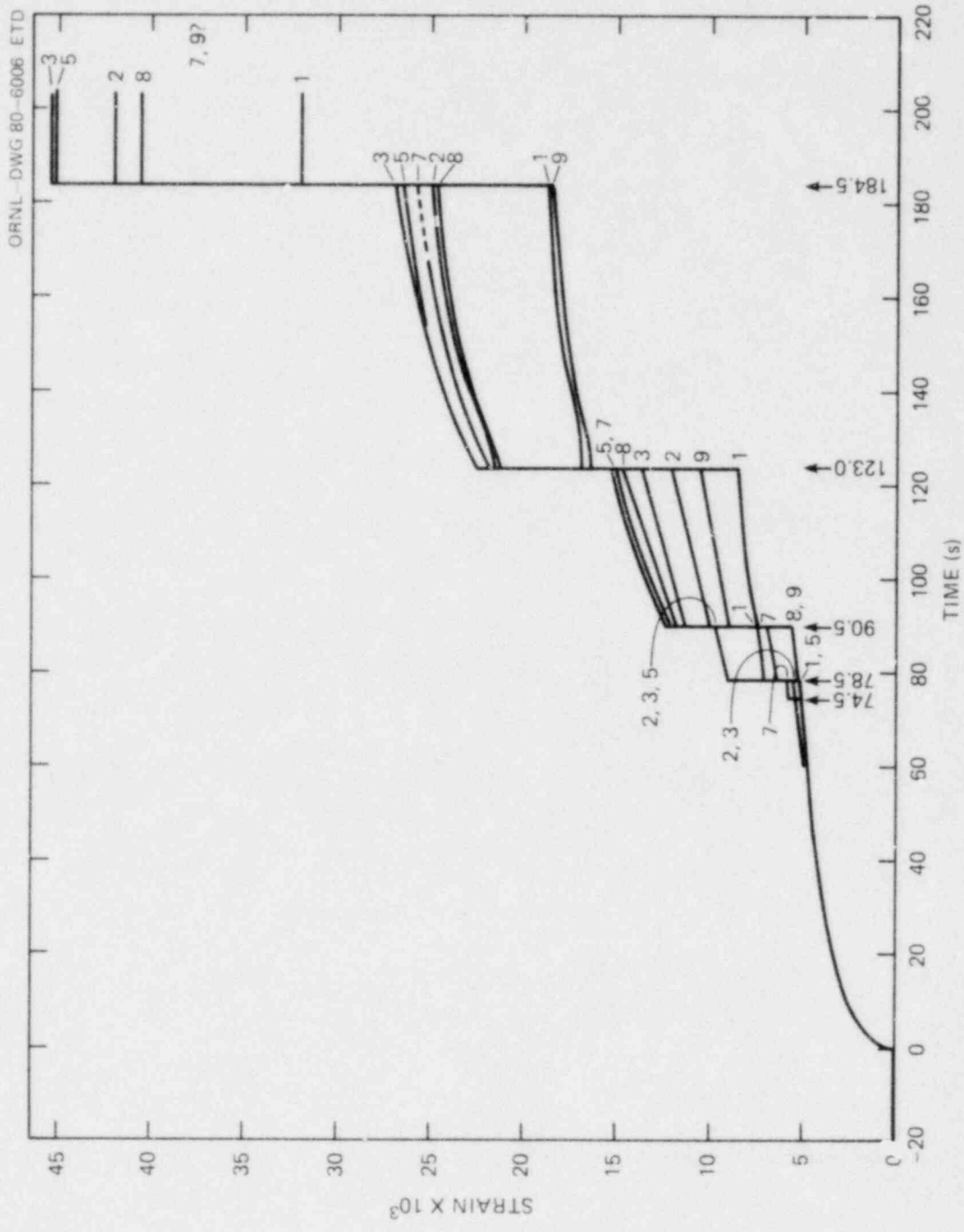

Fig. 4.2. COD data for TSE-5A.

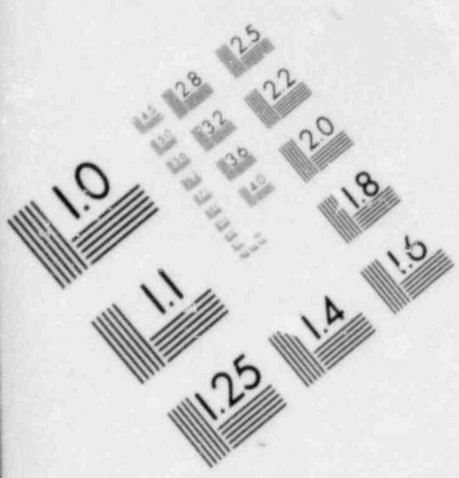

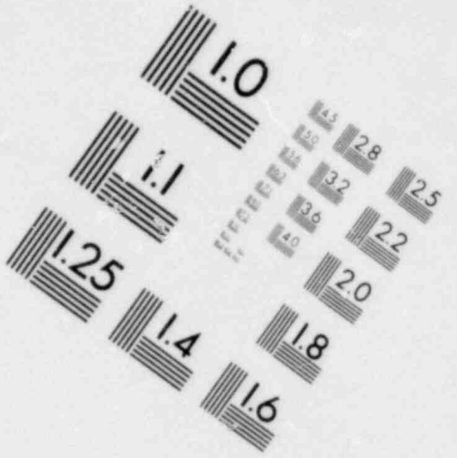

IMAGE EVALUATION
TEST TARGET (MT-3)

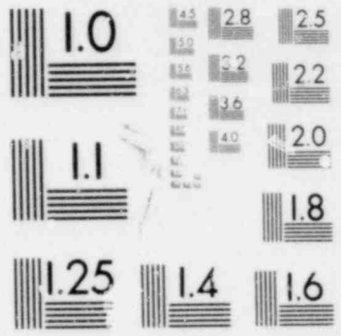

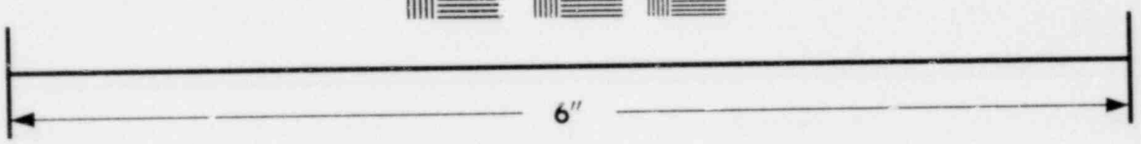

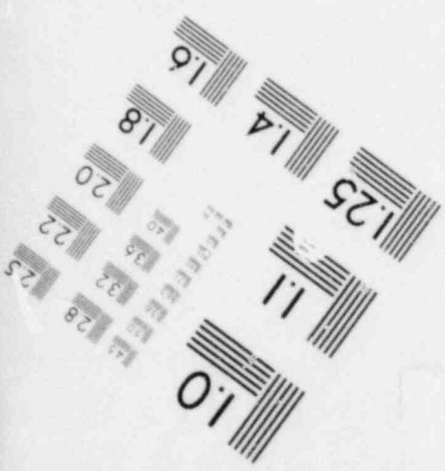

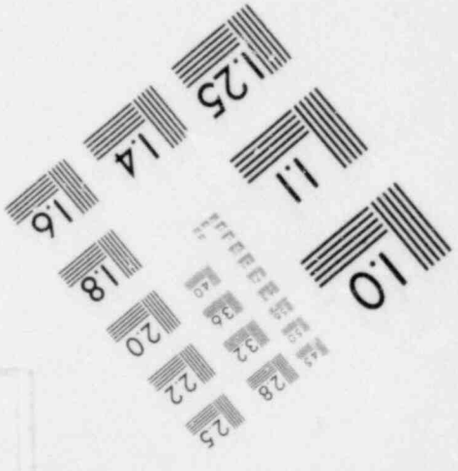

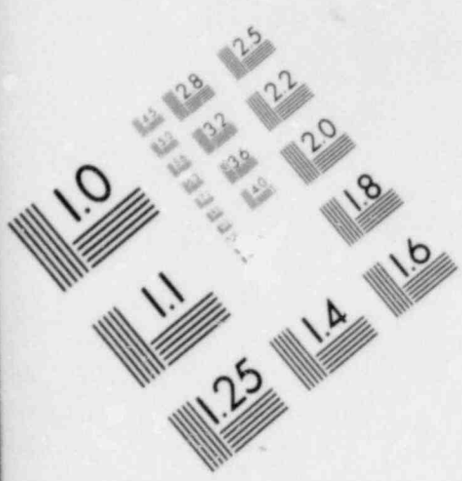

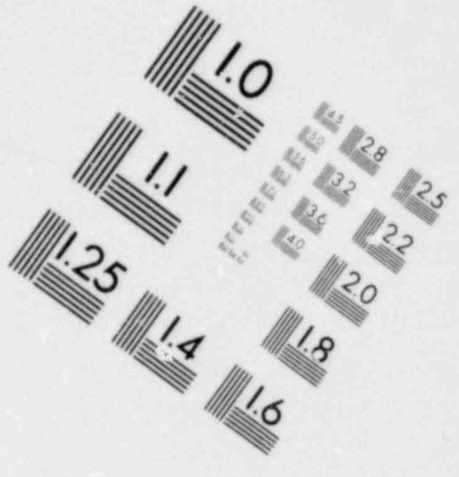

IMAGE EVALUATION TEST TARGET (MT-3)

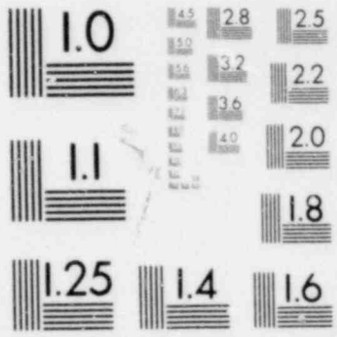

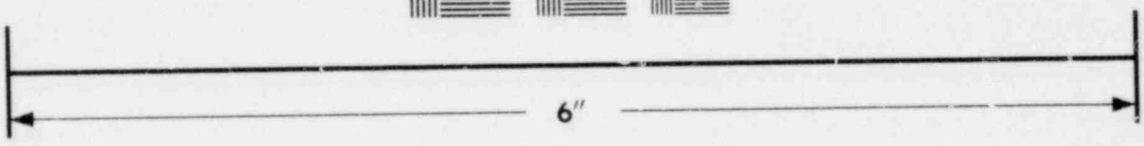

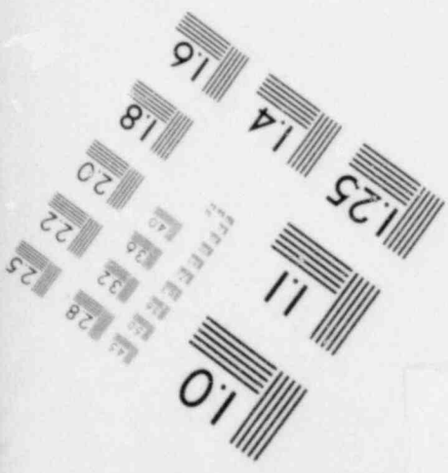

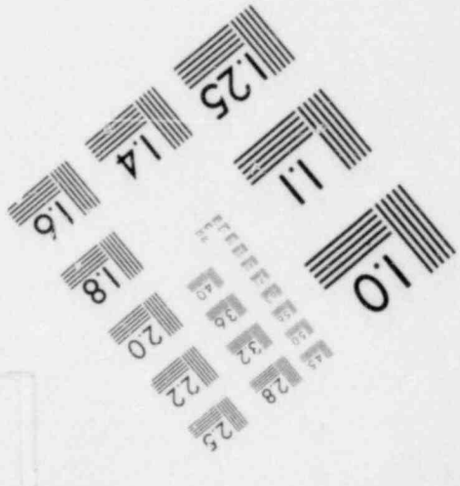

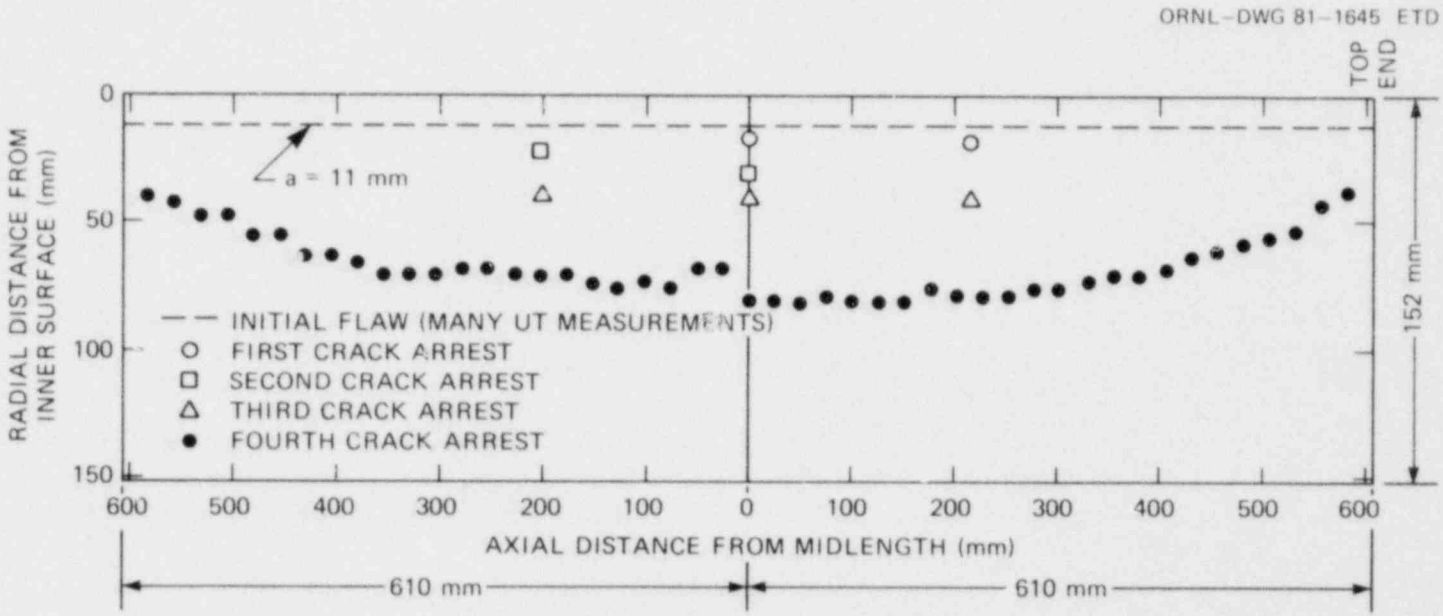

Fig. 4.3. Crack depths determined with UT instrumentation.

Before proceeding with the posttest analysis, the crack depths corresponding to each of the events must be determined as closely as possible. The UT measurements tend to be very localized, and thus crack-tip irregularities can introduce false readings relative to an effective local average crack depth. A better indication of the latter value can be obtained from an interpretation of COD in terms of crack depth. This interpretation relates crack depth to COD by means of a posttest finite-element analysis. The COD-gauge output was accurately converted to actual COD by means of a COD-gauge calibration,[2] and a temperature-effect bias in the COD-gauge output was removed by normalizing the data to the directly measured final flaw depth. The calculated COD vs-crack-depth curves for each of the times at which initiation-arrest events took place are shown in Fig. 4.4, and the crack depths derived therefrom are listed in Table 4.2. As indicated, some differences exist between the UT- and COD-derived values.

Another source of crack-depth data was the fracture surface, a composite of which is shown in Fig. 4.5. This photograph shows that the initial flaw was quite uniform in depth from end to end of the test cylinder. However, as shown schematically in Fig. 4.6, the first initiation-arrest event covered only the upper two-thirds of the crack length, while the second event covered the bottom two-thirds, leaving a continuous and symmetrical crack front for the third initiation event. The third and fourth events were full-length and symmetrical.

In Fig. 4.5, a fifth event is indicated in the central region of the test cylinder. This distinct event was detected with the UT instrumentation but not with the COD gauges. According to the UT data, the time between the fourth and fifth events was <900 μs. The intermediate arrest event was probably caused by dynamic effects (cycling K_I) and will not be treated as a separate event in the posttest static analysis.

As deduced from the fracture surfaces, crack depths near midlength for the four major events are included in Table 4.2. Crack depths deduced from COD and fracture appearance, both of which represent local averages, agree quite well.

The number of initiation-arrest events taking place during TSE-5A agrees with the pretest analysis (Fig. 4.1), but the times at which the events actually took place were earlier than calculated. This analysis indicates that the thermal shock was more severe than that used for the pretest analysis and/or that the actual material toughness was less than that used in the pretest analysis. As planned (Fig. 4.7), the thermal shock was more severe than that assumed for the pretest analysis (that achieved during TSE-5), and apparently the toughness was less than assumed, as will be discussed later.

The toughness curves used in the pretest analysis are shown in Fig. 4.8 (Ref. 1). The K_{Ic} curve represents the lower bound of 50 1T-CT data points, while the K_{Ia} curve is a mean curve through 6 data points obtained from 6 × 6 × 1 in. wedge-loaded crack-arrest specimens.

Posttest analyses of TSE-5A were made using the measured test cylinder temperatures shown in Fig. 4.9. The results of such an analysis, which used the toughness curves in Fig. 4.8, are shown in Fig. 4.10, a set of critical-crack-depth curves that includes the actual path of events. Observations are that the initiation and arrest events fall to

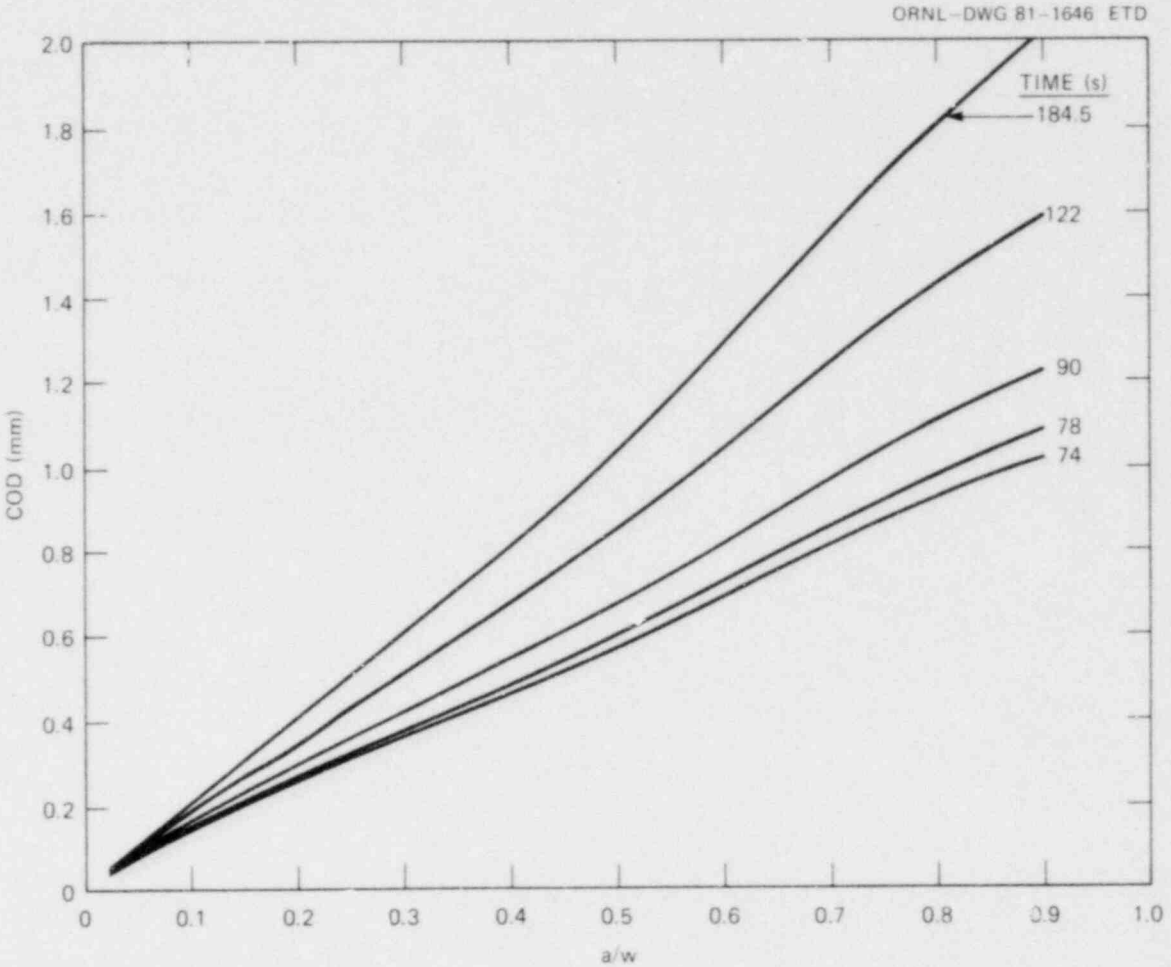

Fig. 4.4. Calculated COD at inner surface vs fractional crack depth for TSE-5A.

Table 4.2. Estimated crack depths near midlength of test cylinder for TSE-5A

Event No.	Event	Time (s)	Crack depth (mm)		
			UT	COD	Fracture surface
1	Initiation	78.5	11	12	11
	Arrest		17	21	23
2	Arrest	90.5	31	30	30
3	Arrest	123.0	41	48	48
4	Arrest	184.5	81	81	81

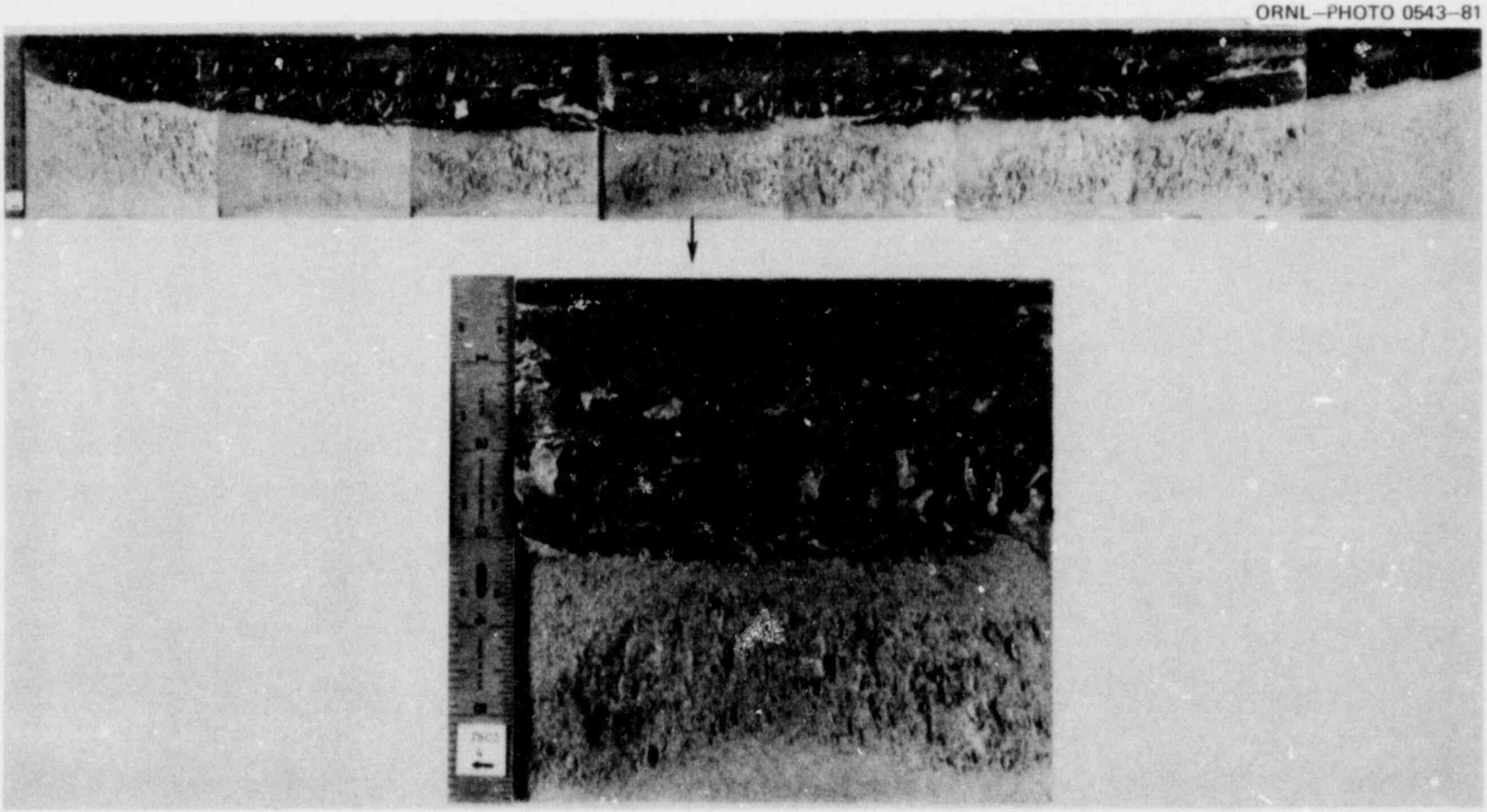

Fig. 4.5. TSE-5A fracture surface.

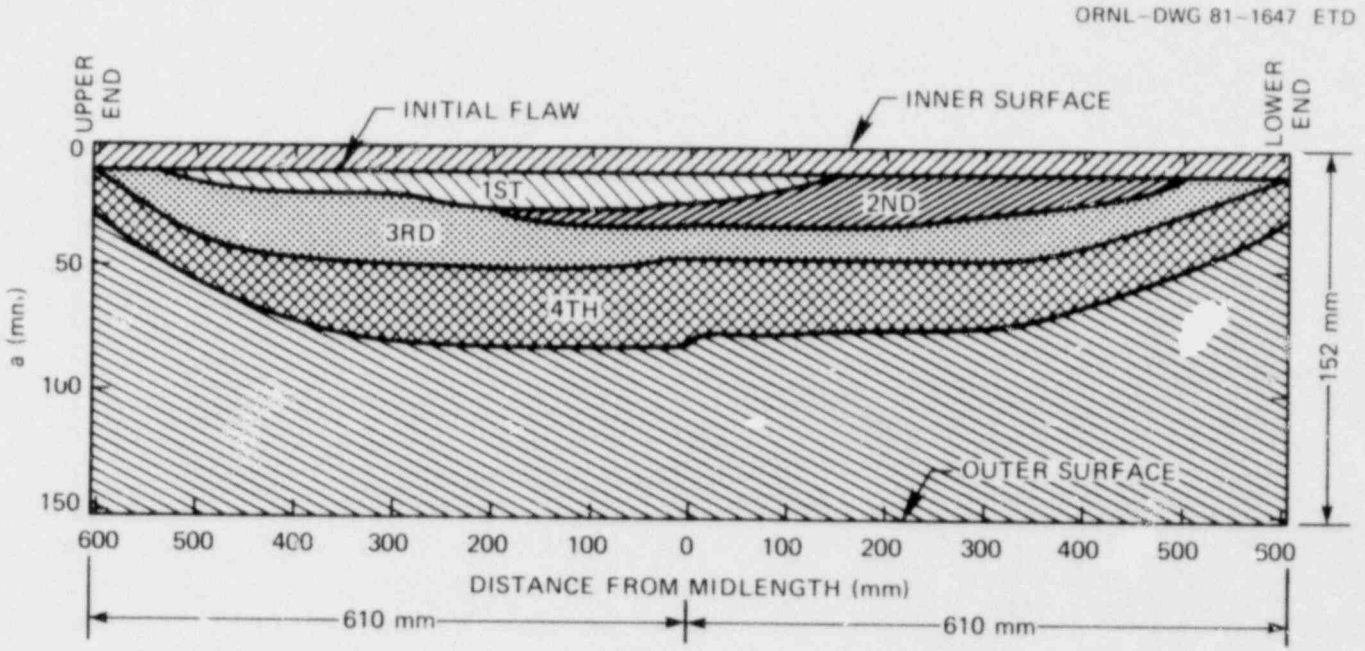

Fig. 4.6. Schematic cross section of TSE-5A test-cylinder wall, showing four-step progression of long axial flaw as deduced from fracture surfaces.

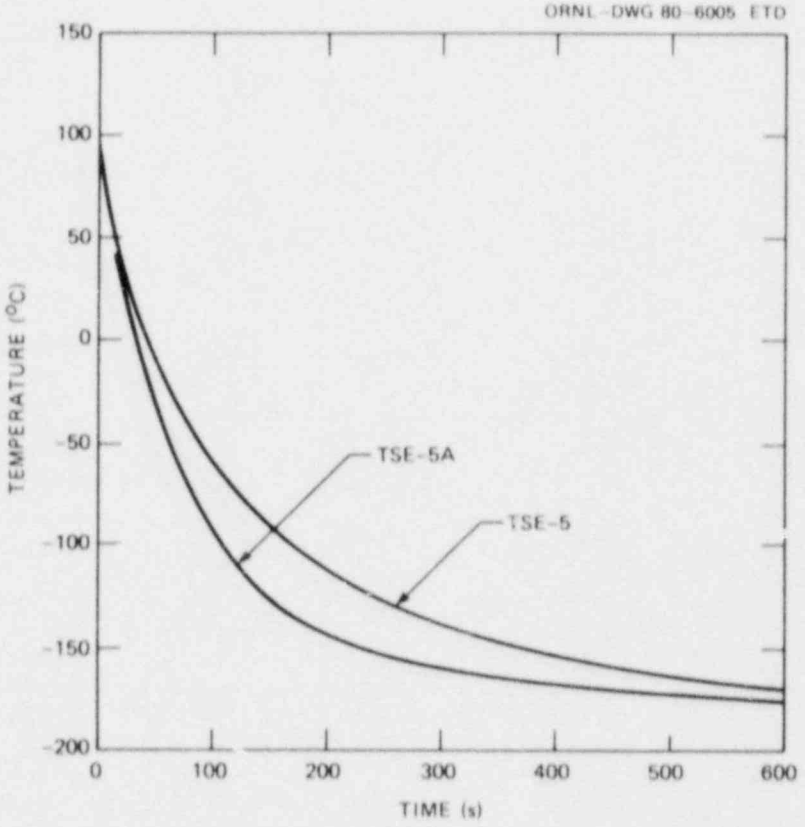

Fig. 4.7. Comparison of inner-surface (a/w = 0.0083) quench rates for TSE-5 (assumed for TSE-5A pretest analysis) and TSE-5A.

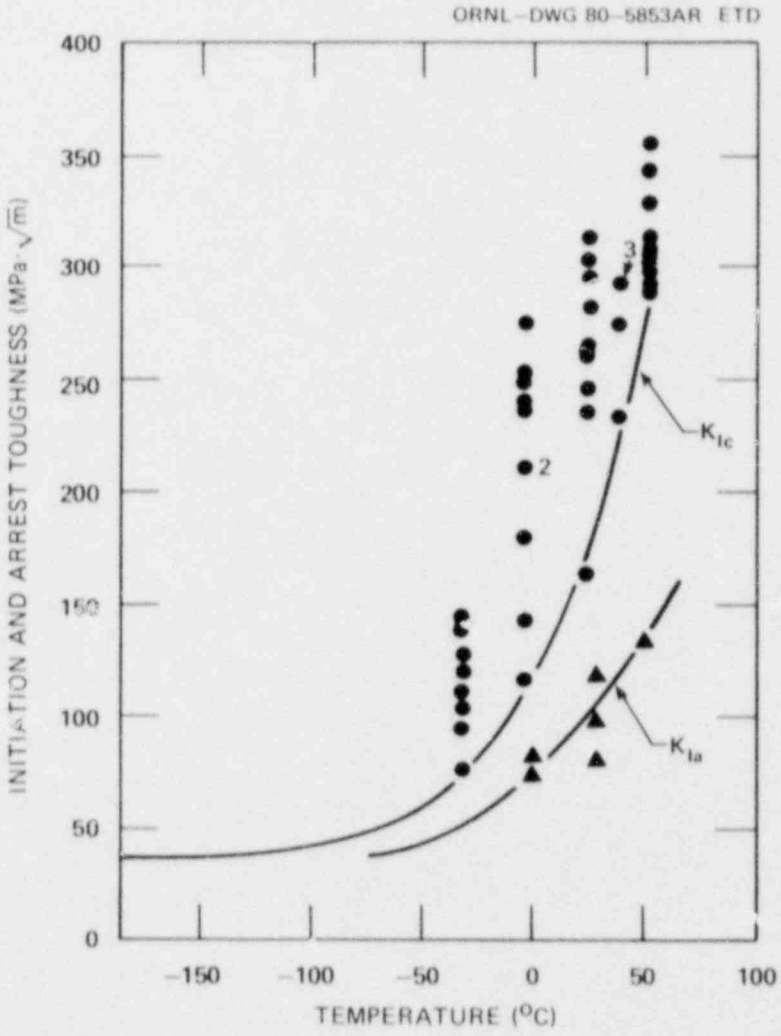

Fig. 4.8. Initiation and arrest toughness data for TSC-2 prolongation tempered at 677°C.

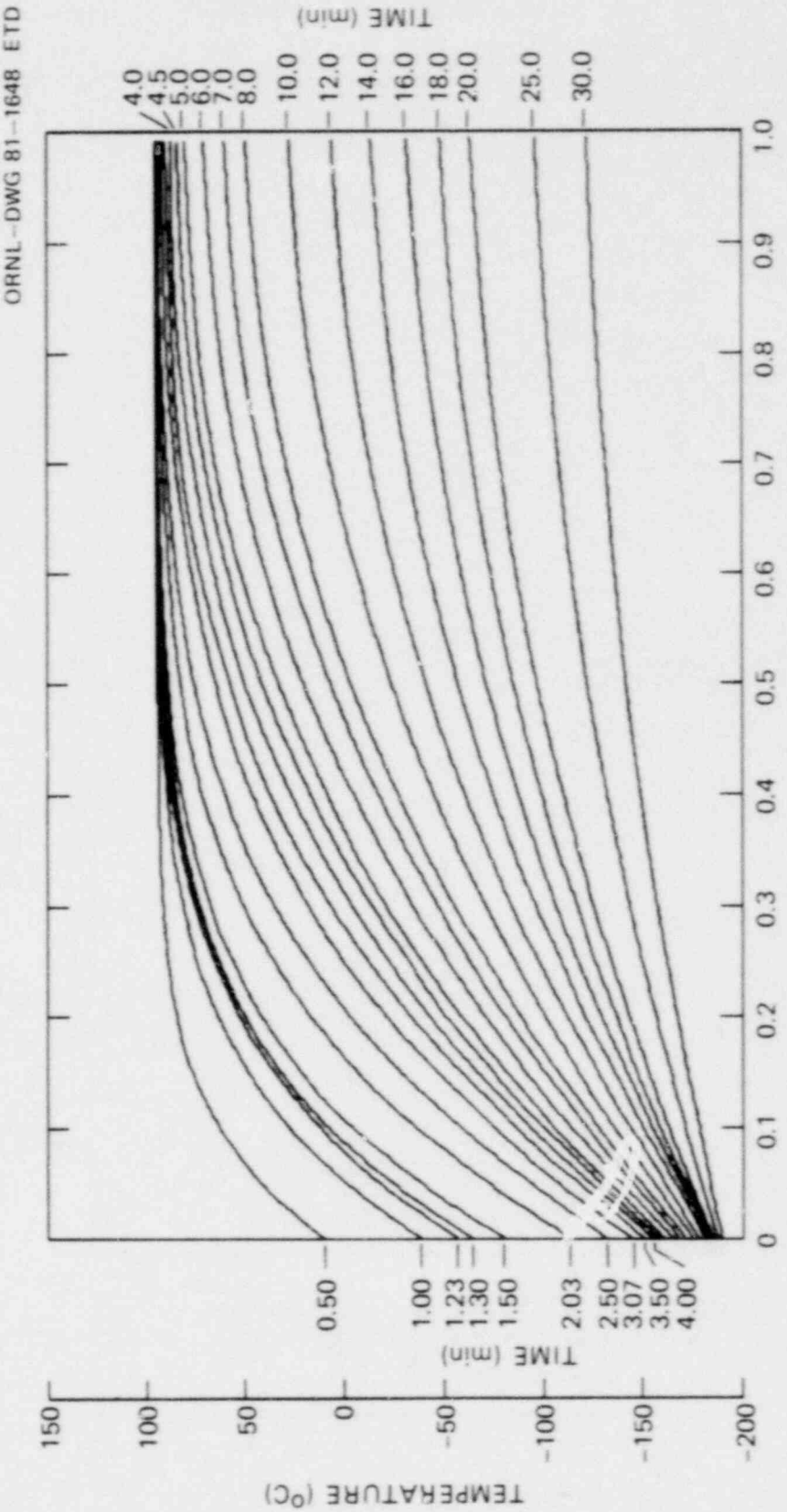

Fig. 4.9. Temperature distributions in wall of TSC-2 during TSE-5A.

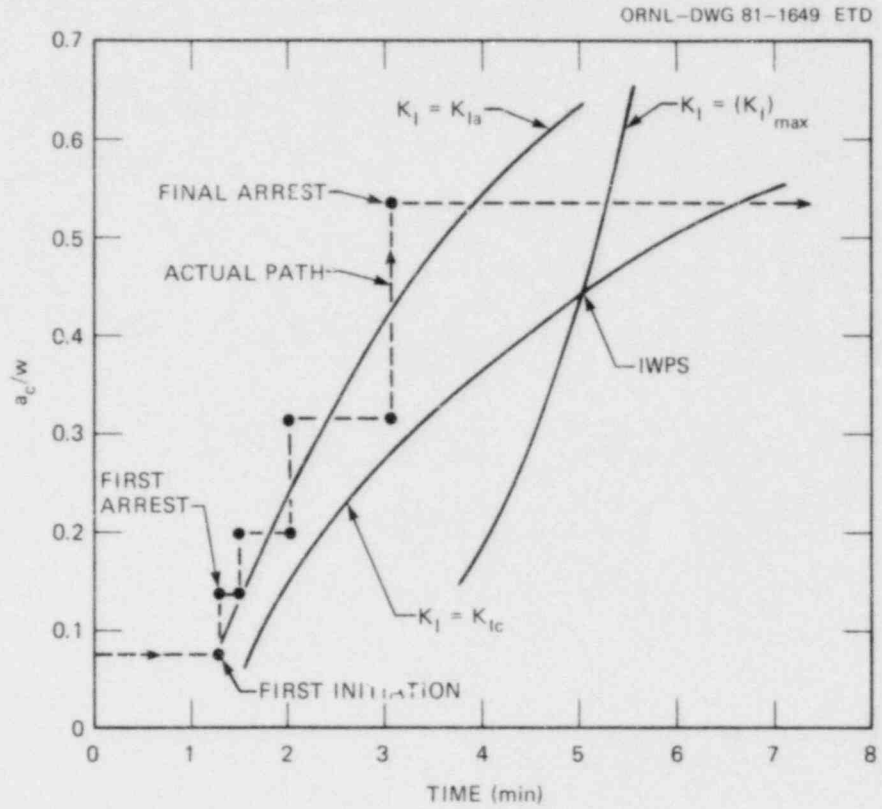

Fig. 4.10. Critical-crack-depth curves for TSE-5A based on toughness curves in Fig. 4.8.

the left of their respective calculated initiation and arrest curves, indicating that the actual fracture- and arrest-toughness values were less than those indicated by the curves in Fig. 4.8. This behavior is also indicated by comparing the calculated K_I values corresponding to the actual initiation-arrest events with the curves in Fig. 4.8. Such a comparison is made in Fig. 4.11, which indicates that a better fit would be obtained by using the modified curves, shifted to the right by ~22 K. This modification was made for a second posttest analysis, and the results are shown in Fig. 4.12. The agreement is much better, of course, indicating that our extensive pretest material-characterization study did not properly define the effective fracture toughness and arrest toughness for the test cylinder.

Another important observation is illustrated in Fig. 4.12: a fifth initiation event was prevented by warm prestressing, and $(K_I/K_{Ic})_{max}$ corresponding to the final crack depth (a/w = 0.53) was 2.3. This value of $(K_I/K_{Ic})_{max}$ is large enough to compensate for all uncertainties in the experiment and analysis and thus provides assurance that warm prestressing was, in fact, effective in preventing additional initiation events.

Another important result of TSE-5A is indicated in Fig. 4.13, which is a plot of K_I vs a/w for each of the four times at which initiation-arrest events took place. Included in this figure is the actual path of

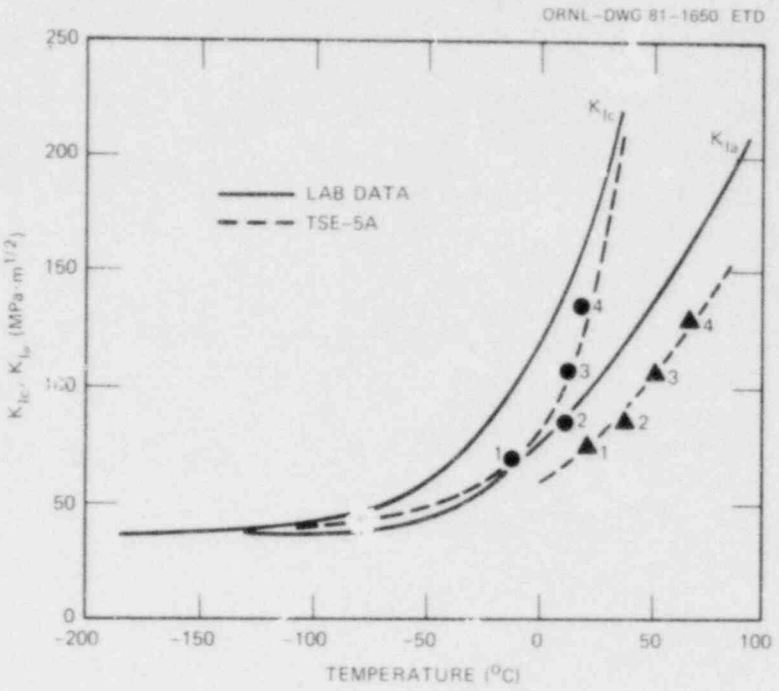

Fig. 4.11. Comparison of K_{Ic} and K_{Ia} values deduced from TSE-5A (based on COD crack-depth data) with laboratory data presented in Fig. 4.8.

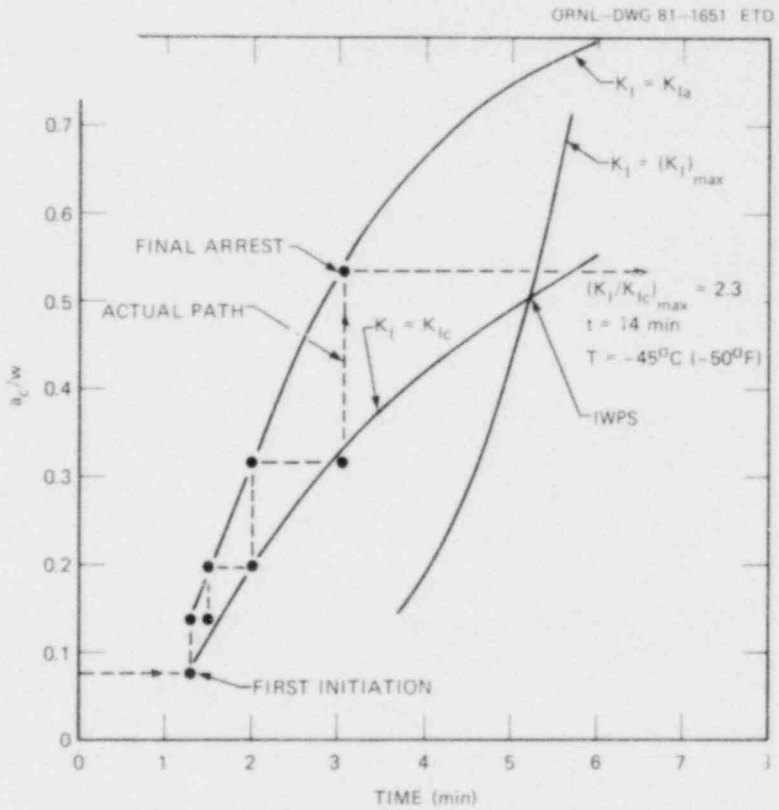

Fig. 4.12. Posttest critical-crack-depth curves for TSE-5A using modified toughness curves in Fig. 4.11 and crack depths based on COD.

events, and as indicated, the first arrest event took place in a rising K_I field.

This preliminary posttest analysis of TSE-5A indicates that all objectives of TSE-5A were accomplished. A summary of data pertaining to the results of TSE-5A is included in Table 4.3.

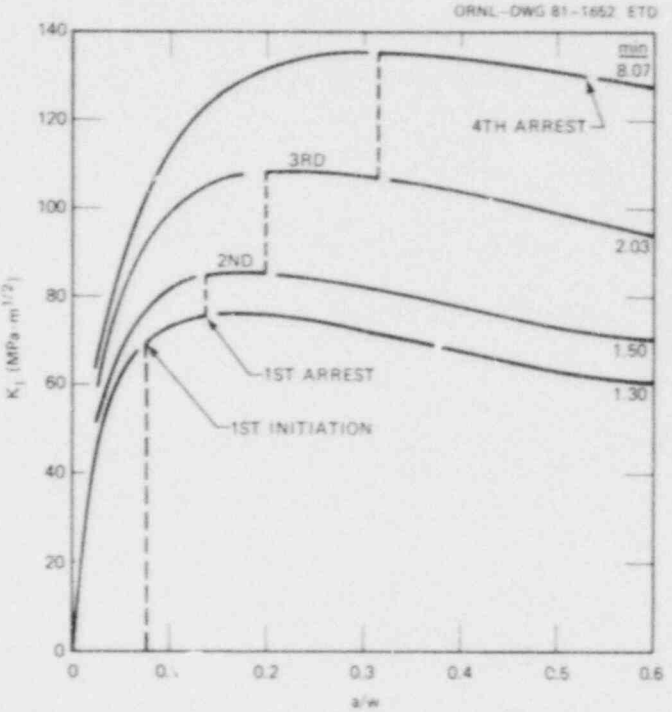

Fig. 4.13. K_I vs a/w and t for TSE-5A

Table 4.3. Summary of data for TSE-5A using crack depths estimated from COD data

Time (s)	Event	a/w	K_I (MPa·$\sqrt{m}$)	Temperature (°C)
78.5	1st initiation	0.076	70	−11
90.5	2nd initiation	0.137	85	12
123.0	3rd initiation	0.198	108	13
184.5	4th initiation	0.318	135	21
78.5	1st arrest	0.139	76	22
90.5	2nd arrest	0.199	86	38
123.0	3rd arrest	0.314	107	51
184.5[a]	4th arrest	0.535	130	67

[a] K_I/K_{Ic} reached a maximum value of 2.3 at ~14 min.

4.2 The OCA Code

A computer program referred to as OCA is being developed to provide a 2-D LEFM analysis of a PWR vessel under essentially any thermal-pressure transient loading condition. Input to OCA will include primary-system coolant temperature and pressure transients, and the output will include a set of critical-crack-depth curves indicating the behavior of long axial flaws during the entire transient. A block diagram of the major functions of OCA is shown in Fig. 4.14.

To facilitate its use, OCA has been made as simple as possible. The K_I values are calculated using superposition by simply summing K_I values for appropriately weighted point loads on the crack face. The K_I values for the unit-point loads (K_I*) were calculated for a specific set of PWR vessel dimensions using our finite-element analysis and are incorporated in the code. If one wishes to analyze a different vessel size, a new set of K_I* values will have to be calculated and inserted.

The particular method for calculating K_I has been proposed and used by others, but there has always been some question regarding its accuracy, particularly for deep flaws. As a check on accuracy, the method was used with our PWR loss-of-coolant-accident-emergency-core-cooling (LOCA-ECC) reference model to calculate fractional crack depths ranging up to 0.9. The exact same mesh was used for calculating the unit-point load K_I values as was used for the previous finite-element fracture mechanics calculations that considered the stress distribution through the entire wall. As calculated by the two methods, K_I values were within 1.0% for all crack depths and for all times in the LOCA-ECC transient. This was a very severe test of the superposition method, and apparently the method works very well.

The OCA code is now operational but is not quite ready for distribution.

4.3 Thermal Shock Materials Characterization

W. J. Stelzman D. A. Canonico

The drop-weight nil-ductility temperature T_{NDT} with CA-oriented* P-3 drop-weight specimens[3] from a segment of the thermal-shock vessel TSC-2 prolongation (TSP-2) is 10°C. The segment had received the same temper treatment as the vessel TSC-2: 4 h at 679°C and cooled in air. The RT_{NDT} was also determined with CA-oriented Charpy-V specimens (C_V) using the 68-J energy and 0.89-mm lateral expansion criteria set forth in Section III, Subsection NB, Article NB-2330 of the *ASME Boiler and Pressure Vessel Code*.[4] An example of an application has been described previously.[5] The results from C_V tests are listed in Table 4.4 and then shown in Fig. 4.15.

The lowest temperature at which the criteria were met by the required three C_V specimens was 10°C (T_{C_V} = 10°C); therefore, the RT_{NDT} from the C_V specimens would be −23°C. Selecting the higher of the two temperatues, (−23 and 10°C), then the $RT_{NDT} = T_{NDT}$ = 10°C.

---

*Circumferential-axial.

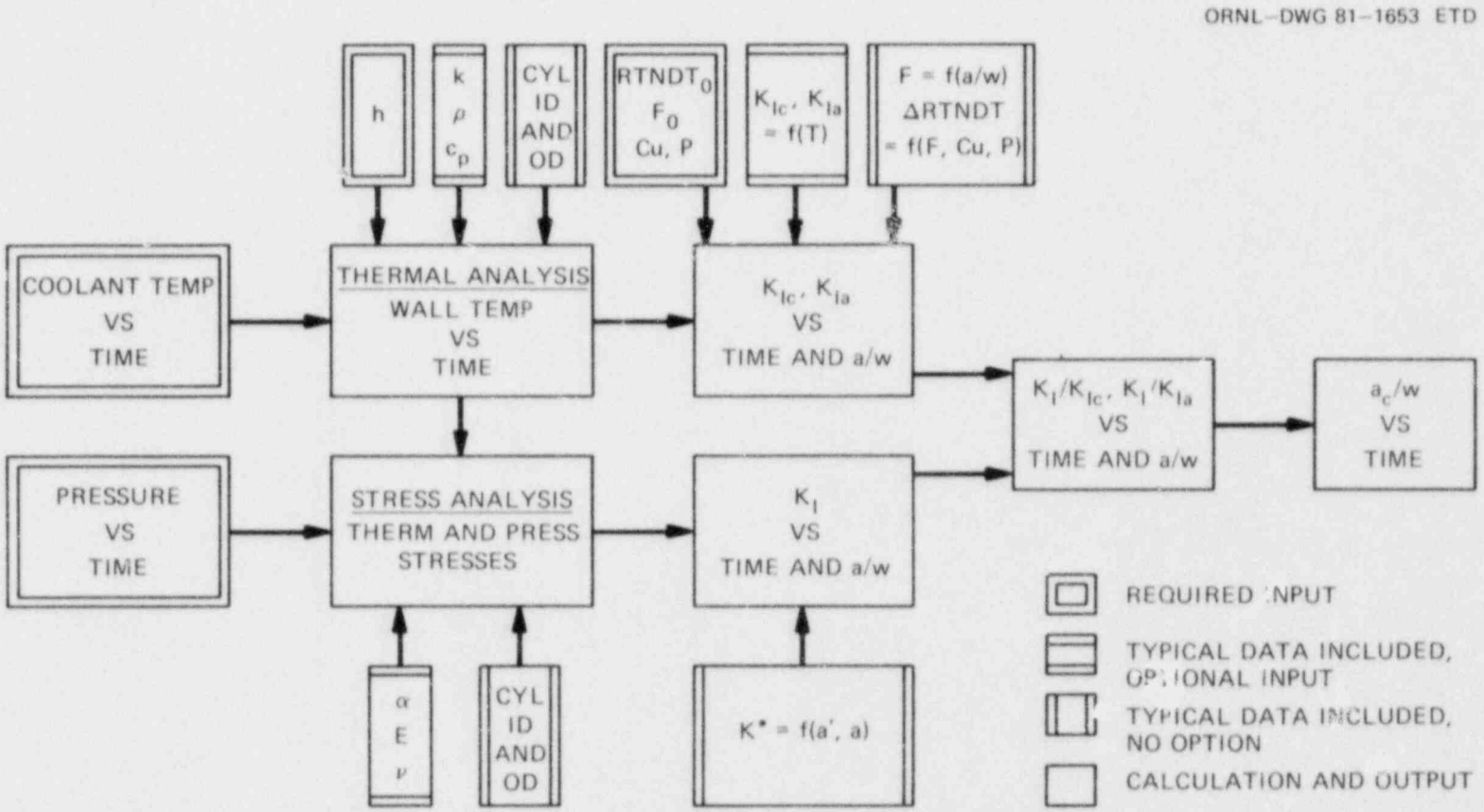

Fig. 4.14. Main components of OCA.

Table 4.4. Test results used in determining the reference NDT of thermal-shock prolongation TSP-2

Test temperature [°C (°F)]	Energy[a] (J)	Lateral expansion[a] (mm)
−46 (−50)	30	0.38
−18 (0)	83.5	0.99
−18 (0)	55.5	0.58
−12 (10)	70	0.71
−12 (10)	76	0.89
−12 (10)	27	0.20
−7 (20)	87.5	1.04
−7 (20)	89	1.07
−7 (20)	44.5	0.56
10 (50)[b]	91.5	1.09
10 (50)[b]	114	1.45
10 (50)[b]	68	0.89
23 (73)	114	1.45
43 (110)	140	1.63
54 (130)	92	1.45
54 (130)	134	1.68
66 (150)	154	1.93
79 (175)	155	2.03

[a]CA-oriented specimens.

[b]Lowest temperature at which three specimens exceeded 68 J and 0.89 mm.

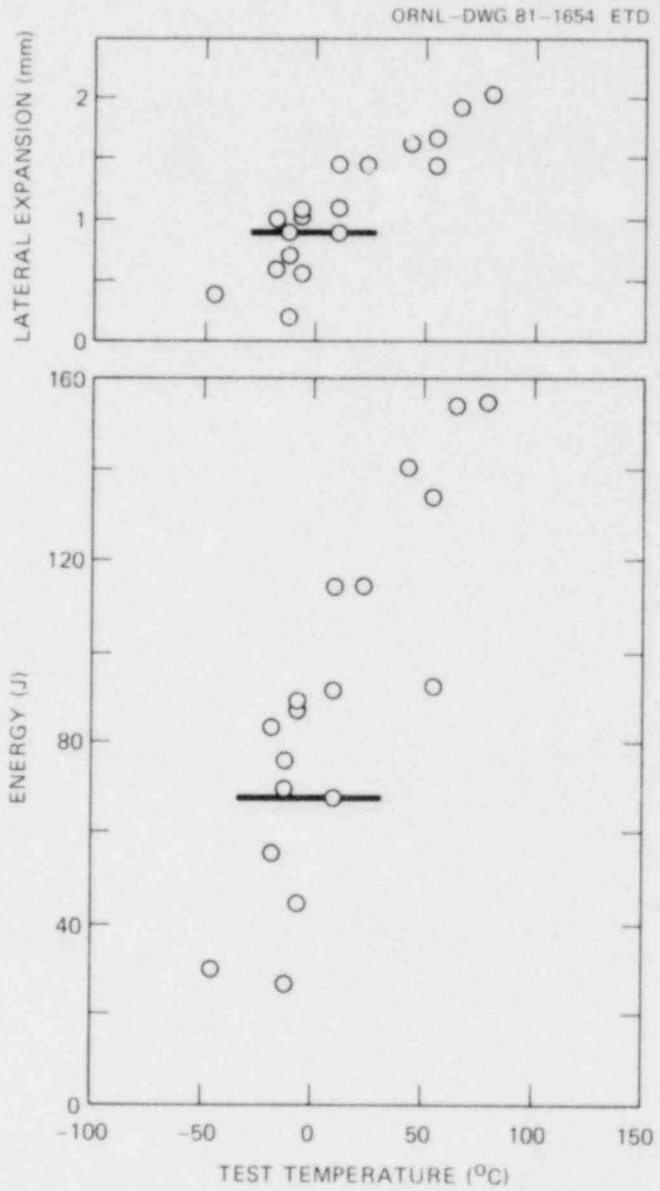

Fig. 4.15. Charpy-V impact properties of "as-quenched" prolongation TSP-2 (SA-508) after tempering at 678°C for 4 h and cooling in air.

References

1. R. D. Cheverton et al., "Thermal Shock Investigations," *Heavy-Section Steel Technology Program Quart. Prog. Rep. July–September 1980*, NUREG/CR-1806 (ORNL/NUREG/TM-419), pp. 31–52.

2. R. D. Cheverton et al., "Thermal Shock Investigations," *Heavy-Section Steel Technology Program Quart. Prog. Rep. October–December 1979*, NUREG/CR-1305 (ORNL/NUREG/TM-380), pp. 63–67.

3. "Conducting Drop-Weight Test to Determine Nil-Ductility Transition Temperature of Ferritic Steels, ASTM Designation: E 208-69," *Annual Book of ASTM Standards*, Part 10, 1977 Edition.

4. ASME Boiler and Pressure Vessel Code, *Section III, Division 1, Nuclear Power Plant Components*, 1977 Edition and Addenda, American Society of Mechanical Engineers, New York.

5. W. J. Stelzman and D. A. Canonico, "Characterization of the V-9 Prolongation," *Heavy-Section Steel Technology Program Quart. Prog. Rep. October–December 1978*, NUREG/CR-0656 (ORNL/NUREG/TM-298), pp.40–43.

5. PRESSURE VESSEL INVESTIGATIONS

5.1 Intermediate Test Vessel V-8A

P. P. Holz R. H. Bryan

Nearly all work under subcontract for Phase I has been completed by Babcock and Wilcox (B&W), Alliance Research Center, Alliance, Ohio, and by B&W Nuclear Equipment Division (NED), Barberton, Ohio.[1] We are only lacking results from two out of four J-integral tests and some procedural documentation toward Phase II and III work. Vessel V-8, the prolongation, and associated materials have been shipped to Barberton, Ohio. Informal agreement with B&W was achieved on all aspects of the contract for vessel preparation, and the DOE-approved contract document has been sent to B&W. A mid-January 1981 review meeting is scheduled to formally wind up Phase I and to officially start on the vessel repair and characterization phases of the work.

Results from the B&W trial weldment (V8-42) made in the Barberton shops are in close agreement with earlier B&W preliminary welds (V8-22) made in Alliance and meet contract prerequisites as shown in Table 5.1. The weld chemistry for the as-made welds is listed in Table 5.2.

In an attempt to achieve 100% shear in the 66 to 93°C range, B&W Alliance also tried an automatic submerged-arc (ASA) weld (V8-Q2) with what was thought to be more favorable welding-wire composition. The weld had about the same onset of upper-shelf temperature of 93°C but with a higher fracture-appearance transition temperature. Additional work with the alternate wire was subsequently discontinued.

The materials and the welding parameters for the trial weld (V8-42) were essentially the same as for the preliminary weld V8-22, except that a lower heat input was used for the trial weld, in the hope that the transition temperature would be diminished slightly. Thirty-three CVN impact specimens of this weld were tested in the temperature range from −73 to 260°C. Twenty-one of these tests were in the range from 66 to 121°C, in which the onset of upper shelf lies. On the basis of 100% shear fracture appearance, the upper shelf is attained between 93 and 99°C. On the basis of this information, we decided that 120°C would be an appropriate upper-shelf temperature for the testing of tensile and J-integral specimens from the trial weld.

Preliminary analyses of data from J tests of two 25-mm-thick compact specimens without corrections give an average value of $J_{Ic} = 63.3\ kJ \cdot m^{-2}$. Preliminary values of the parameters C and n in the power law expression for the J-integral,

$$J = C(\Delta a)^n ,$$

were determined from a fit of data over the range of crack extension Δa,

Table 5.1. Vessel V-8A, B&W automated submerged-arc low-upper-shelf weldment experimentation[a]

Designation	Target range	Base metal – V80	Weld – V8-22	Trial weld V8-42
Material thickness, mm	152	152	95	152
Welding current, A			575 ± 15	475 ± 25
Welding voltage, V ac			32 ± 2	32 ± 2
Welding speed, mm/min			305 ± 1	305 ± 1
Heat input, kJ/mm	2950		3620	2990
Postweld heat treatment				
Heatup rate, maximum, K/h	55	78	28	83
Hold temperature and time, °C, h	566–593, 48–52	588, 58	580, 50	584, 52
Cooling rate, K/h	5–7.5	6.9	6.1	5.1
CVN impact tests				
Upper-shelf absorbed energy, 93 to 149°C, J	54–68 47.5–74.5 acceptable		57.2	57.6
Upper-shelf lateral expansion, 93 to 149°C, mm			1.2	1.3
Temperature at upper shelf (100% shear), °C	66–93		107	99
Tensile properties				
Yield stress, room temperature, MPa	448–620	452.0	461.3	459.9
Yield stress, 121°C, MPa		413.7		419.9
Ultimate stress, room temperature, MPa	551–690	598.5	564.7	568.1
Ultimate stress, 121°C, MPa		549.5		519.2
Elongation, room temperature, %	18 min.	27.8	24.7	25.8
Elongation, 121°C, %		25.7		24.3
Reduction in area, room temperature, %		70.4	54.4	55.3
Reduction in area, 121°C, %		70.0		53.5
Drop-weight NDT temperature, °C				–12

[a]Base material – SA 533, grade B, Class 1
Wire – 1/8-in.-diam Mn-Mo-Ni type SFA 5.23, EF-2
Flux – 75% Linde 60 and 25% Linde 80
Preheat – 149°C min; interpass 260°C max

Table 5.2. Comparison of chemical analyses for B&W ASA welds V8-22 and V8-42

(averaged wt %)

Element	Weld V8-22	Weld V8-42
C	0.06	0.05
Mn	1.61	1.50
P	0.024	0.028
S	0.017	0.016
Si	0.65	0.66
Cr	0.04	0.05
Ni	0.61	0.62
Mo	0.48	0.45
Cu	0.29	0.27
Sn	0.025	0.026
V	0.009	0.007
Al	0.003	0.006

from ~0.15 to 13 mm:

$$C = 112.224\ kJ \cdot m^{-2}/(mm)^n ,$$

$$n = 0.407925 .$$

Note that this uncorrected J-R curve lies within the range of data from upper-shelf tests of 41-mm specimens of irradiated high-copper welds reported by Loss of the Naval Research Laboratory.[2] Thus, apparently the special seam weld material in vessel V-8A will have ductile tearing properties roughly representative of irradiated low-upper-shelf welds, as had been hoped. In terms of V-8A test objectives, a lower J-R curve would permit a more useful experiment. Tests of larger J-specimens in the characterization phase of B&W's work may indicate such behavior.

5.2 Pressurized Thermal Shock Studies

R. H. Bryan G. C. Robinson

Behavior of flaws in pressure vessels has been studied experimentally in the HSST Program in structures of essentially full-scale thickness for

pressure loads, thermal shock loads, and combined residual stress-pressure loads. The series of thermal-shock experiments in the HSST Program is concerned principally with investigating and demonstrating the application of LEFM to thermal shocks without pressure, while the intermediate vessel test series has been concerned with pressure without thermal shock. The intermediate vessel tests involved elastic-plastic as well as LEFM behavior.

In nuclear power plants, several hypothetical or real system failures would impose concurrent pressure- and thermal-shock loadings on the reactor pressure vessel. Examples are steam line breaks and small primary-coolant line breaks. The combined loading imposed by such accidents has all of the complexities introduced by the nonstatic nature of the thermal stress and by temporal and spatial variations of fracture toughness. The combined loading also introduces the potential for a variety of situations that have not been investigated experimentally. For example, loading sequences may occur that promote intermittent episodes of cleavage and tearing modes of crack growth.

One should be able to evaluate vessel integrity for many combined load situations with methods already confirmed by HSST experiments. However, cases probably exist for which pressurized thermal shock tests would be essential to the development of reliable, but not overly conservative, evaluation methods.

In view of the potential applications of pressurized-thermal-shock test results, preliminary design concepts are being formulated; thermal, stress, and fracture analyses are being made for the purpose of determining the scope and feasibility of large-scale experiments.

The ensuing discussion will briefly review concepts that have been considered, problems that were analyzed, and reasons for adopting or discarding some test concepts.[3-6]

The nozzle-corner region of a vessel was initially of interest because of its high stress concentration. Consequently, high stress-intensity factors could probably be achieved under nominally large-scale elastic conditions in an intermediate vessel test. Furthermore, there was a secondary interest in using a pressurized-thermal-shock test facility for the study of nozzle-corner crack initiation under pressure and thermally induced fatigue.[3] Exploratory calculations of stress-intensity factors were carried out by a combination of finite-element and influence-function computer codes for pressurized thermal shock.[4] Thermally induced cyclic stresses pertinent to fatigue crack formation were estimated by methods of classical thermoelasticity.

Both types of nozzle-corner experiments, that is, pressurized thermal shock and thermal fatigue, would require a test system that could deliver coolant to the nozzle-corner region at appropriate temperatures and high flow rates. Coolant temperatures would have to vary to a few hundred Kelvins below the mean vessel temperature; the coolant pressure would be approximately test vessel pressure, ~70 to 100 MPa. Preliminary design studies indicated that pumps of the type and capacity required would be expensive and dimensional tolerances in the flow distribution apparatus at the nozzle corner would be stringent.

The possibility of attaining crack propagation by cleavage in a nozzle-corner pressurized thermal shock was discussed by Corwin[5] on the basis

of ADINAT-ADINA-BIGIF calculations by Bryson et al.[4] Corwin illustrated the uncertainties of crack initiation with test pressures at, or below, intermediate test vessel design pressure (66.9 MPa) and with test vessel material of typical toughness. Initiation could be realized at higher pressure, still in the large-scale elastic range; but it is doubtful that a suitable coolant pump with a design pressure above ~70 MPa could be acquired.

The preliminary flawed nozzle-corner analyses were by no means sufficiently thorough, accurate, or pessimistic to preclude useful tests in that geometry. Other factors, however, favored placing the flaw in the barrel of the test vessel. The cylindrical barrel section is geometrically similar to the part of a reactor pressure vessel that is of greatest concern in a pressurized-thermal-shock accident. Fracture analysis of the cylindrical region should also be simpler; possibly the same methods of analysis could be applied to both test vessel and reactor vessel evaluation.

Crack initiation in pressurized-thermal-shock tests of a cylinder with the flaw on the inside surface would be more difficult to achieve than in tests of flawed nozzle corners. Because of the absence of stress concentrations, the pressure contribution to the stress-intensity factor K_I would be smaller in the cylinder. Furthermore, the surface area subjected to the thermal shock would probably have to be larger. These difficulties have been avoided by the acceptance of the outside surface as a suitable site for a flaw subjected to thermal shock.

Advantages of this choice of the flaw site are numerous. Thermal shocks may be induced on the outside surface of a test vessel by coolant at low pressure, that is, without the use of high-pressure canned rotor pumps, which are the most expensive components in the facility for testing nozzle-corner flaws. Because the coolant loop can operate near atmospheric pressure, apparently a testing facility can be designed and used with greater flexibility. Much higher coolant flow rates are practicable, allowing the cooling of larger surface areas. Furthermore, design of the cooling system has no influence whatsoever on the choice of test pressures. Finally, fabrication or implantation of a test zone having special material properties is practicable.

In a pressurized-thermal-shock test, an outside flaw in a cylinder with a thermal shock administered to the outside surface is believed to be an adequate representation of conditions that would obtain in the flawed region of a reactor pressure vessel. This is so even though the outside flaw extends into a rising pressure-stress gradient and a falling one in the case of the inside flaw. This gradient is small in reactor vessels. In a pressurized-thermal-shock test, stress gradients are most likely dominated by the thermal stress in the early phases of the transient. Consequently, the outside flaw–outside shock arrangement does not appear to impose serious limitations.

References

1. R. H. Bryan and P. P. Holz, "Intermediate Test Vessel V-8A," *Heavy-Section Steel Technology Program Quart. Prog. Rep. July–September 1980,* NUREG/CR-1806 (ORNL/NUREG/TM-419), p. 53.

2. F. J. Loss, "Toughness and Ductile Shelf Properties of Irradiated Low-Shelf Weld Metals," Nuclear Regulatory Commission 8th Water Reactor Safety Research Information Meeting, Gaithersburg, Md., Oct. 27–31, 1980.

3. R. H. Bryan et al., "Pressurized Thermal Shock and Thermal Fatigue Tests," *Heavy-Section Steel Technology Program Quart. Prog. Rep. July–September 1979,* NUREG/CR-1197 (ORNL/NUREG/TM-370), p. 51.

4. J. W. Bryson, B. R. Bass, and R. H. Bryan, "Determination of K-Factors for Nozzle-Corner Flaws Under Combined Pressure-Thermal Loading," *Heavy-Section Steel Technology Program Quart. Prog. Rep. April–June 1980,* NUREG/CR-1627 (ORNL/NUREG/TM-401), pp. 3–5.

5. W. R. Corwin, "Pressurized Thermal Shock Studies," *Heavy-Section Steel Technology Program Quart. Prog. Rep. April–June 1980,* NUREG/CR-1627 (ORNL/NUREG/TM-401), p. 58.

6. W. R. Corwin, "Pressurized Thermal Shock Studies," *Heavy-Section Steel Technology Program Quart. Prog. Rep. April–June 1980,* NUREG/CR-1806 (ORNL/NUREG/TM-419), pp. 53–60.

CONVERSION FACTORS[a]

SI unit	English unit	Factor
mm	in.	0.0393701
cm	in.	0.392701
m	ft	3.28084
m/s	ft/s	3.28084
kN	lb_f	224.809
kPa	psi	0.145038
MPa	ksi	0.145038
$MPa \cdot \sqrt{m}$	ksi $\sqrt{in.}$	0.910048
J	ft-lb	0.737562
K	°F or °R	1.8
kJ/m^2	$in.-lb/in.^2$	5.71015
$W \cdot m^{-2} \cdot K^{-1}$	$Btu/hr-ft^2-°F$	0.176110
$T(°F) = 1.8\ T(°C) + 32$		

[a]Multiply SI quantity by given factor to obtain English quantity.

NUREG/CR-1941
ORNL/NUREG/TM-437
Dist. Category RF

Internal Distribution

1. L. G. Berggren
2. S. E. Bolt
3-7. R. H. Bryan
8. J. W. Bryson
9. D. A. Canonico
10. R. D. Cheverton
11. J. M. Corum
12. W. R. Corwin
13. W. B. Cottrell
14. J. R. Dougan
15. W. L. Greenstreet
16. R. C. Gwaltney
17. P. P. Holz
18. S. K. Iskander
19. K. K. Klindt
20. J. G. Merkle
21. C. A. Mills
22. S. E. Moore
23. F. R. Mynatt
24. D. J. Naus
25. F. H. Neill
26. G. C. Robinson
27-28. T. W. Robinson
29. G. M. Slaughter
30. J. E. Smith
31. W. J. Stelzman
32. H. E. Trammell
33-37. G. D. Whitman
38. Patent Office
39. Central Research Library
40. Document Reference Section
41-42. Laboratory Records Department
43. Laboratory Records (RC)

External Distribution

44. C. Z. Serpan, Reactor Safety Research, Nuclear Regulatory Commission, Washington, DC 20555
45. M. Vagins, Reactor Safety Research, Nuclear Regulatory Commission, Washington, DC 20555
46. Office of Assistant Manager for Energy Research and Development, DOE, ORO, Oak Ridge, TN 37830
47-48. Technical Information Center, DOE, Oak Ridge, TN 37830
49-478. Given distribution as shown in category RF (NTIS — 10)

☆U.S. GOVERNMENT PRINTING OFFICE: 1981-740-062/527